Waves in Random and Complex Media
Vol. 17, No. 3, August 2007, 283–303

Bistatic scattering from one-dimensional random rough homogeneous layers in the high-frequency limit with shadowing effect

N. PINEL*, N. DÉCHAMPS, C. BOURLIER and J. SAILLARD

IREENA, Ecole polytechnique de l'université de Nantes, La Chantrerie, Rue C. Pauc, BP 50609, 44306 Nantes Cedex 3, France

(Received 15 May 2006; in final form 17 December 2006)

Many fast asymptotic models of electromagnetic scattering from a single rough interface have been developed over the last few years, but only a few have been developed on stacks of rough interfaces. The specific case of very rough surfaces, compared to the incident wavelength, has not been treated before, which is the context of this paper. The model starts from the iteration of the Kirchhoff approximation to calculate the fields scattered by a rough layer, and is reduced to the high-frequency limit in order to rapidly obtain numerical results. The shadowing effect, important under grazing angles, is taken into account. The model can be applied to any given slope statistics. Then, the model is compared with a reference numerical method based on the method of moments, which validates the model in the high-frequency limit for lossless and lossy inner media.

1. Introduction

Scattering from dielectric homogeneous layers has many applications, like remote sensing of ocean ice, sand cover of arid regions, or oil slicks on the ocean, and also in optics, like optical studies of thin films and coated surfaces, and treatment of antireflection coatings. The use of fast asymptotic models can be very useful to predict the scattered signal of such systems.

Several models have been developed on rough films where only one surface scatters an incident wave (for example, see [1] and references therein). Only a few asymptotic models have been developed on scattering from stacks of rough interfaces, which is the context of this paper. The first models on this subject were developed for optical applications, for stacks of slightly rough surfaces compared to the incident wavelength [2–4]. One can also quote the small perturbation method (SPM) extended to two interfaces [5], also valid for small roughnesses. However, the mathematical formulation of this method is so complicated that no numerical result has been presented. Soubret *et al*. [6] extended the reduced Rayleigh equations to the case of two slightly rough interfaces. Fuks *et al*. [7–9] developed a model for scattering from a slightly rough surface overlying a strongly rough surface compared to the incident electromagnetic wavelength. Bahar *et al*. have developed the full wave model over more than 30 years for a rough interface, and extended it to the case of two rough interfaces

*Corresponding author. E-mail: nicolas.pinel@univ-nantes.fr

Waves in Random and Complex Media
ISSN: 1745-5030 (print), 1745-5049 (online)
http://www.tandf.co.uk/journals
DOI: 10.1080/17455030701191448

[10]. Simulations have been presented for the monostatic configuration, and for surfaces with rms heights smaller than the wavelength [11]. Using the radiative transfer model, Tjuatja *et al*. [12] presented numerical results of the monostatic scattering coefficient from a stack of two rough interfaces separated by an inhomogeneous medium, modeled as a collection of randomly distributed spheres. In addition, the scattering from each interface is calculated from the asymptotic integral equation method of Fung *et al*. [13, 14]. Nevertheless, this approach seems to be very difficult to implement numerically, and to demand extensive computing time.

The objective of this paper is to obtain a simple mathematical expression of the bistatic scattering coefficient in the high-frequency limit (taking the shadowing effect into account), in order to get a fast method for solving the problem of rough homogeneous layers: it is an extension of the classical geometric optics approximation for one rough interface to the case of several rough interfaces. The starting point of the method is the Kirchhoff approximation (KA) [14–18], applicable to surfaces with large radii of curvature compared to the incident electromagnetic wavelength. The model uses the widely used KA in reflection, but also the KA in transmission [14, 17, 18], which allows one to obtain the fields reflected onto and transmitted through a rough interface. This paper describes the KA applied to a stack of two rough interfaces, in which the KA is iterated for each successive reflection or transmission on the two rough interfaces. To our knowledge, this is the first time that this problem has been investigated: iterating the KA has only been done for multiple scattering from a single rough interface [19–21], and only at order two (second-order scattering). It is applied to strongly rough interfaces to obtain a simple mathematical expression of the bistatic radar cross-section in the high-frequency limit, allowing easy numerical implementation and fast numerical results. The paper focuses on one-dimensional stationary random rough surfaces, and takes the shadowing effect into account [22, 23].

In the second part of the paper, the expressions of the first- and second-order scattered fields are derived with the method of stationary phase (MSP). In the third part, the expressions of the radar cross-sections are derived in the high-frequency limit (using the geometric optics approximation). Then, numerical results are presented and compared with a benchmark method [24, 25] based on the method of moments to validate the model. A comparison between a rough and a plane lower interface is made, and the case of a lossy inner medium is studied.

2. First- and second-order scattered fields derived with the method of stationary phase

The studied system (see figure 1) is composed of a stack of two rough interfaces (Σ_A for the upper interface, Σ_B for the lower interface), separated by an intermediate homogeneous medium Ω_2. The three media Ω_α ($\alpha = \{1, 2, 3\}$), with relative permittivity $\epsilon_{r\alpha}$, are supposed to be non-magnetic (relative permeability $\mu_{r\alpha} = 1$). k_α stands for the wavenumber inside Ω_α ($k_\alpha = k_0\sqrt{\epsilon_{r\alpha}}$, with k_0 the wavenumber in the vacuum). Let E_i be the incident field inside the medium Ω_1, of direction $\hat{\boldsymbol{k}}_{\boldsymbol{i}} = (k_i, q_i)/|k_1| = (\hat{k}_i, \hat{q}_i)$, and of incidence angle θ_i. The incident field on the upper surface at the point A_1 is given by $E_i(\boldsymbol{r}_{\boldsymbol{A_1}}) = E_0 \exp(i\, k_1 \hat{\boldsymbol{k}}_{\boldsymbol{i}} \cdot \boldsymbol{r}_{\boldsymbol{A_1}})$ (the term $\exp(-i\,\omega t)$ is omitted), $\boldsymbol{r}_{\boldsymbol{A_1}} = x_{A_1}\hat{\boldsymbol{x}} + z_{A_1}\hat{\boldsymbol{z}}$, with x_{A_1} and z_{A_1} the abscissa and the elevation of the point A_1, respectively.

The field transmitted into the intermediate medium Ω_2 along the downward propagation direction $\hat{\boldsymbol{k}}_{-,1}$ (angle $\theta_{-,1}$ with subscript $-$ representing the downward direction) is reflected onto the lower surface at the point B_1 along the upward propagation direction $\hat{\boldsymbol{k}}_{+,\mathbf{1}}$ (angle $\theta_{+,1}$ with subscript $+$ representing the upward direction), and then reflected onto the upper surface at the point A_2 and so on. Thus, multiple reflections of the field inside Ω_2 occur, successively

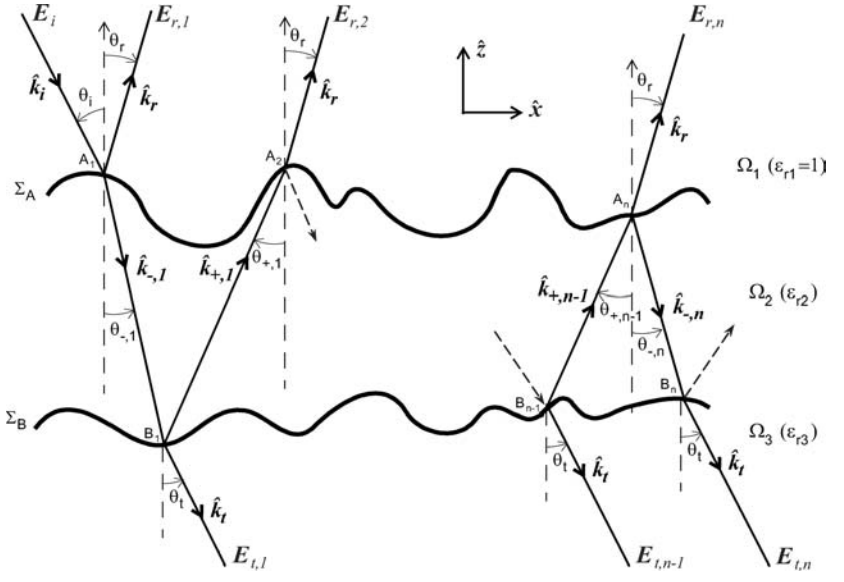

Figure 1. Multiple scattering from two rough interfaces Σ_A and Σ_B. The points on the upper surface Σ_A are denoted as $\{A_1, A_2, \ldots, A_n\}$, whereas the points on the lower surface Σ_B are denoted as $\{B_1, B_2, \ldots, B_n\}$. θ_i is the incidence angle, and θ_r, θ_t are the scattering angles in reflection and transmission, respectively, measured with respect to the vertical axis $\hat{\mathbf{z}}$. The positive sense is defined as clockwise.

on the lower interface Σ_B at the point B_k ($k \in \{1, \ldots, n-1\}$), and then on the upper interface Σ_A at the point A_{k+1}. This system can be seen as a rough dielectric waveguide. Only the first two scattered fields in reflection, $E_{r,1}$ and $E_{r,2}$, and the first in transmission, $E_{t,1}$, will be treated in detail in this paper. Nevertheless, we will see that the higher orders can be calculated at any order in reflection as well as in transmission.

$E_{r,1}$ and $E_{r,2}$ denote the first- and second-order scattered fields inside the incident medium Ω_1. They are observed in the reflection direction $\hat{\boldsymbol{k}}_{\boldsymbol{r}} = (k_r, q_r)/|k_1| = (\hat{k}_r, \hat{q}_r)$, with a scattering angle θ_r. $E_{t,1}$ denotes the first-order scattered field inside the inner medium Ω_3. It is observed in the transmission direction $\hat{\boldsymbol{k}}_{\boldsymbol{t}} = (k_t, q_t)/|k_3| = (\hat{k}_t, \hat{q}_t)$, with a scattering angle θ_t. $\theta_i \in [-\pi/2; 0]$, and $\theta_{-,1}, \theta_t, \theta_{+,1}, \theta_r \in [-\pi/2; +\pi/2]$, are measured with respect to the vertical axis $\hat{\boldsymbol{z}}$, where the positive sense is defined as clockwise. With $\hat{\boldsymbol{k}}_{-,\mathbf{1}} = (k_{-,1}, q_{-,1})/|k_2| = (\hat{k}_{-,1}, \hat{q}_{-,1})$ and $\hat{\boldsymbol{k}}_{+,\mathbf{1}} = (k_{+,1}, q_{+,1})/|k_2| = (\hat{k}_{+,1}, \hat{q}_{+,1})$, we have

$$\begin{cases} \hat{\boldsymbol{k}}_{\boldsymbol{i}} = (-\sin\theta_i, -\cos\theta_i) \\ \hat{\boldsymbol{k}}_{\boldsymbol{r}} = (+\sin\theta_r, +\cos\theta_r) \end{cases} \qquad \begin{cases} \hat{\boldsymbol{k}}_{-,\mathbf{1}} = (-\sin\theta_{-,1}, -\cos\theta_{-,1}) \\ \hat{\boldsymbol{k}}_{+,\mathbf{1}} = (+\sin\theta_{+,1}, +\cos\theta_{+,1}). \end{cases} \tag{1}$$

In order to determine the fields $E_{r,1}$, $E_{t,1}$, and $E_{r,2}$, the iteration of the Kirchhoff approximation (KA) is used for both interfaces at each scattering point (in reflection or transmission). It is valid in the restrictive case of interfaces whose radii of curvature are larger than the incident wavelength λ_0. The field on every point of the considered surface can then be approximated by the field that would be present on its tangent plane. Thus, the Snell–Descartes laws and the Fresnel coefficients can be applied locally, on every point of the considered surface. Moreover, the method of stationary phase (MSP) is used on the two interfaces, at each scattering point. Based on the KA, it assumes that the major contribution of the scattered field comes from regions of the rough surface in the vicinity of the (stationary phase) specular points of the rough surface, whose direction is given by the local normal to the surface and the incidence angle.

In the first subsection, the general principle of the method is exposed from the case of the first-order scattered field $E_{r,1}$. In the second subsection, $E_{t,1}$ and $E_{r,2}$ are derived for a rough lower interface, and in the last one they are derived for a plane lower interface.

2.1. *General principle of the method*

First, the fields scattered in reflection and transmission from the upper interface Σ_A at the point A_1 are expressed from the classical Kirchhoff–Helmholtz integral equations with the use of the Kirchhoff approximation [23]. Then, using the Weyl representation of the Green function, one can express the scattered fields at any point of the two media, that is to say Ω_1 for the field scattered in reflection, and Ω_2 for the field scattered in transmission. The scalar two-dimensional Weyl representation of the Green function $G_\alpha^{MM'} = G_\alpha(\boldsymbol{r_M}, \boldsymbol{r_{M'}})$, for a wave propagating from a point M to a point M' in the medium Ω_α, is defined as

$$G_\alpha^{MM'} = \frac{i}{4} H_0^{(1)}(k_\alpha \|\boldsymbol{r_{M'}} - \boldsymbol{r_M}\|) = \frac{i}{4\pi} \int_{-\infty}^{+\infty} \frac{d\,\hat{k}_{MM'}}{\hat{q}_{MM'}}\, e^{i\,k_\alpha \hat{\boldsymbol{k}}_{\boldsymbol{MM'}} \cdot \boldsymbol{r_{MM'}}}, \tag{2}$$

where $\hat{k}_{MM'} = \hat{\boldsymbol{k}}_{\boldsymbol{MM'}} . \hat{\boldsymbol{x}}$, and $\hat{q}_{MM'} = \hat{\boldsymbol{k}}_{\boldsymbol{MM'}} . \hat{\boldsymbol{z}}$, with

$$\hat{q}_{MM'} = \begin{cases} \left[1 - \hat{k}_{MM'}^2\right]^{1/2} & \text{if } \|\hat{\boldsymbol{k}}_{\boldsymbol{MM'}}\| \le 1 \\ i\left[\hat{k}_{MM'}^2 - 1\right]^{1/2} & \text{if } \|\hat{\boldsymbol{k}}_{\boldsymbol{MM'}}\| > 1, \end{cases} \tag{3}$$

where $\boldsymbol{r_M} = x_M \hat{\boldsymbol{x}} + z_M \hat{\boldsymbol{z}}$, with x_M and z_M the abscissa and the elevation of the point M, respectively. Let us note that the Weyl representation of the Green function is valid for far-field as well as for near-field propagations. The formalism in equation (2), which uses the scalar product $\hat{\boldsymbol{k}}_{\boldsymbol{MM'}} \cdot \boldsymbol{r_{MM'}}$ inside the exponential (similar to the formalism expressed by Bahar *et al.* [19]) is equivalent to the classical form using absolute values over the heights z_M and $z_{M'}$, $|z_{M'} - z_M|$ in [26]. When the scattered field is observed in the far-field zone at the point P, the two-dimensional scalar Green function can be expressed by the following asymptotic form:

$$G_\alpha^{MP} \simeq \frac{i}{4} \left(\frac{2}{\pi k_\alpha r}\right)^{1/2} \exp\{i[k_\alpha(r - \hat{\boldsymbol{k}}_{\boldsymbol{s}} \cdot \boldsymbol{r_M}) - \pi/4]\}, \tag{4}$$

where r is the distance of P from an arbitrary origin. For our configuration, $\hat{\boldsymbol{k}}_{\boldsymbol{s}} = \hat{\boldsymbol{k}}_{\boldsymbol{r}}$ if $\alpha = 1$, and $\hat{\boldsymbol{k}}_{\boldsymbol{s}} = \hat{\boldsymbol{k}}_{\boldsymbol{t}}$ if $\alpha = 3$.

Then, using the Kirchhoff–Helmholtz integral equation under the Kirchhoff approximation and the asymptotic Green function in equation (4), and adding the surface illumination function $\Xi(\boldsymbol{r_{A_1}})$, one can express the first-order scattered field $E_{r,1}$ in the incident medium in the far-field zone. Moreover, using the method of stationary phase, the expression can be simplified to

$$\begin{aligned} E_{r,1}(\boldsymbol{r_P}) = {} & \left(\frac{k_1}{2\pi r}\right)^{\frac{1}{2}} \exp[i(k_1 r - \pi/4)]\, r_{12}\left(\chi_{ri}^0\right) f(\hat{\boldsymbol{k}}_{\boldsymbol{i}}, \hat{\boldsymbol{k}}_{\boldsymbol{r}}, \boldsymbol{n}_{\boldsymbol{ri}}^{\boldsymbol{0}}) \\ & \times \int_{-L_0/2}^{+L_0/2} \Xi(\boldsymbol{r_{A_1}})\, \exp(-i k_1 \hat{\boldsymbol{k}}_{\boldsymbol{r}} \cdot \boldsymbol{r_{A_1}})\, E_i(\boldsymbol{r_{A_1}})\, d\, x_{A_1} \end{aligned} \tag{5}$$

with $\Xi(\boldsymbol{r_{A_1}}) = 1$ if the point A_1 corresponding to $\boldsymbol{r_{A_1}}$ is illuminated, and the rays emanating from both the transmitter and the receiver do not cross the surface; $\Xi(\boldsymbol{r_{A_1}}) = 0$ otherwise. L_0 is the illuminated surface length, $f(\hat{\boldsymbol{k}}_{\boldsymbol{i}}, \hat{\boldsymbol{k}}_{\boldsymbol{r}}, \boldsymbol{n}_{\boldsymbol{ri}}) = \boldsymbol{n}_{\boldsymbol{ri}} . (\hat{\boldsymbol{k}}_{\boldsymbol{r}} - \hat{\boldsymbol{k}}_{\boldsymbol{i}})/2$ is obtained from the projection of the incidence and reflection-scattering vectors onto the local normal to the surface $\boldsymbol{n}_{\boldsymbol{ri}} = -\gamma_{ri}\, \hat{\boldsymbol{x}} + \hat{\boldsymbol{z}}$ (defined as being directed upward), with γ_{ri} its associated slope. r_{12} is the Fresnel reflection coefficient, with χ_{ri} the local incidence angle.

With the method of stationary phase, in a general way, let $\hat{\boldsymbol{k}}_{\mathbf{1}}$ represent the incidence unit wave vector inside the medium Ω_α, $\hat{\boldsymbol{k}}_{\mathbf{2}}$ the reflection unit wave vector inside Ω_α, and $\boldsymbol{n}_{\boldsymbol{r1}} = -\gamma_{r1}\,\hat{\boldsymbol{x}}+\hat{\boldsymbol{z}}$ the local normal to the considered surface (defined as being directed upward), with γ_{r1} its associated slope. Then, one can write the projection term as $f(\hat{\boldsymbol{k}}_{\mathbf{1}}, \hat{\boldsymbol{k}}_{\mathbf{2}}, \boldsymbol{n}_{\boldsymbol{r1}}) \equiv f(\hat{\boldsymbol{k}}_{\mathbf{1}}, \hat{\boldsymbol{k}}_{\mathbf{2}}, \boldsymbol{n}^{\mathbf{0}}_{\boldsymbol{r1}}) = [1-(\hat{k}_2\hat{k}_1+\hat{q}_2\hat{q}_1)]\,/\,(\hat{q}_2-\hat{q}_1)$, and the local incidence angle $\chi_{r1} \equiv \chi^0_{r1} = -(\theta_2-\theta_1)/2$ (θ_1, θ_2 are oriented angles). The latter is the argument of the Fresnel reflection coefficient $r_{\alpha\beta}$, defined in H and V polarizations as, respectively,

$$r^H_{\alpha\beta}\left(\chi^0_{r1}\right) = \frac{\sqrt{\epsilon_{r\alpha}}\,\cos\chi^0_{r1} - \sqrt{\epsilon_{r\beta}-\epsilon_{r\alpha}\,\sin^2\chi^0_{r1}}}{\sqrt{\epsilon_{r\alpha}}\,\cos\chi^0_{r1} + \sqrt{\epsilon_{r\beta}-\epsilon_{r\alpha}\,\sin^2\chi^0_{r1}}}, \tag{6}$$

$$r^V_{\alpha\beta}\left(\chi^0_{r1}\right) = -\frac{\epsilon_{r\beta}\,\cos\chi^0_{r1} - \sqrt{\epsilon_{r\alpha}}\sqrt{\epsilon_{r\beta}-\epsilon_{r\alpha}\,\sin^2\chi^0_{r1}}}{\epsilon_{r\beta}\,\cos\chi^0_{r1} + \sqrt{\epsilon_{r\alpha}}\sqrt{\epsilon_{r\beta}-\epsilon_{r\alpha}\,\sin^2\chi^0_{r1}}}. \tag{7}$$

2.2. *Derivation of the scattered fields for a rough lower interface*

To obtain the higher-order scattered fields ($E_{t,1}$, $E_{r,2}$, $E_{t,2}$, $E_{r,3}$, etc.), the principle to be used is exactly the same, and one has to iterate this 'procedure'. For example, to obtain the first-order transmitted scattered field $E_{t,1}$, one first determines the field scattered in transmission from the upper interface at the point A_1 using the Kirchhoff–Helmholtz integral equation under the KA, and the field at the point B_1 using the Weyl representation of the Green function. Then, this procedure is iterated, that is to say the field at the point B_1 can be considered as an incident field on the lower interface at B_1, and the scattered field in transmission at this point can be derived using the Kirchhoff–Helmholtz integral equation under the KA, and then the transmitted field $E_{t,1}$ inside Ω_3 in the far-field zone is derived using the asymptotic Green function in equation (2).

Then, the field $E_{t,1}$, scattered by the rough layer into the lower medium Ω_3 in the far-field zone, results from the scattering in transmission through the surface Σ_A at the point A_1 into the medium Ω_2, and the scattering in transmission through the surface Σ_B at the point B_1 into the medium Ω_3. Taking the surfaces illumination functions $\Xi(\boldsymbol{r}_{\boldsymbol{A_1}})$ and $\Xi(\boldsymbol{r}_{\boldsymbol{B_1}})$ into account and using the MSP, it is expressed as

$$\begin{aligned} E_{t,1} = {} & \frac{k_2}{2\pi}\left(\frac{k_3}{2\pi r}\right)^{\frac{1}{2}} E_0 e^{i(k_3 r-\pi/4)} \int \frac{d\hat{k}_{-,1}}{\hat{q}_{-,1}} dx_{A_1} dx_{B_1}\; \Xi(\boldsymbol{r}_{\boldsymbol{A_1}})\Xi(\boldsymbol{r}_{\boldsymbol{B_1}}) \\ & \times t_{12}\left(\chi^0_{ti}\right) g_{12}\left(\hat{\boldsymbol{k}}_{\boldsymbol{i}}, \hat{\boldsymbol{k}}_{\boldsymbol{-,1}}, \boldsymbol{n}^{\mathbf{0}}_{\boldsymbol{ti}}\right)\; t_{23}\left(\chi^0_{t-,1}\right) g_{23}\left(\hat{\boldsymbol{k}}_{\boldsymbol{-}}, \mathbf{1}, \hat{\boldsymbol{k}}_{\boldsymbol{t}}, \boldsymbol{n}^{\mathbf{0}}_{\boldsymbol{t-,1}}\right) \\ & \times e^{ik_1\hat{\boldsymbol{k}}_{\boldsymbol{i}}\cdot\boldsymbol{r}_{\boldsymbol{A_1}}}\; e^{ik_2\hat{\boldsymbol{k}}_{\boldsymbol{-,1}}\cdot\boldsymbol{r}_{\boldsymbol{A_1B_1}}}\; e^{-ik_3\hat{\boldsymbol{k}}_{\boldsymbol{t}}\cdot\boldsymbol{r}_{\boldsymbol{B_1}}}, \end{aligned} \tag{8}$$

where $\boldsymbol{r}_{\boldsymbol{MM'}} = \boldsymbol{r}_{\boldsymbol{M'}} - \boldsymbol{r}_{\boldsymbol{M}} = (x_{M'}-x_M)\hat{\boldsymbol{x}} + (z_{M'}-z_M)\hat{\boldsymbol{z}}$. In a general way, let $\hat{\boldsymbol{k}}_{\mathbf{1}}$ represent the incidence unit wave vector inside the medium Ω_α, $\hat{\boldsymbol{k}}_{\mathbf{3}}$ the transmission unit wave vector inside the medium Ω_β, and $\boldsymbol{n}_{\boldsymbol{t1}} = -\gamma_{t1}\,\hat{\boldsymbol{x}} + \hat{\boldsymbol{z}}$ the local normal to the considered surface (defined as being directed upward), with γ_{t1} its associated slope. $g_{\alpha\beta}(\hat{\boldsymbol{k}}_{\mathbf{1}}, \hat{\boldsymbol{k}}_{\mathbf{3}}, \boldsymbol{n}_{\boldsymbol{t1}}) = \boldsymbol{n}_{\boldsymbol{t1}}\cdot\hat{\boldsymbol{k}}_{\mathbf{3}}$ is obtained from the projection of the incidence and transmission-scattering vectors onto $\boldsymbol{n}_{\boldsymbol{t1}}$. $t_{\alpha\beta}$ is the Fresnel transmission coefficient, with χ_{t1} the local incidence angle.

Using the MSP, one can write the projection term as $g_{\alpha\beta}(\hat{\boldsymbol{k}}_{\mathbf{1}}, \hat{\boldsymbol{k}}_{\mathbf{3}}, \boldsymbol{n}_{\boldsymbol{t1}}) \equiv g_{\alpha\beta}(\hat{\boldsymbol{k}}_{\mathbf{1}}, \hat{\boldsymbol{k}}_{\mathbf{3}}, \boldsymbol{n}^{\mathbf{0}}_{\boldsymbol{t1}}) = [k_\beta - k_\alpha\,(\hat{k}_3\hat{k}_1 + \hat{q}_3\hat{q}_1)]/(k_\beta\hat{q}_3 - k_\alpha\hat{q}_1)$, and the local incidence angle as $\cos\chi_{t1} \equiv \cos\chi^0_{t1} = \mathrm{sign}[(-\hat{q}_1\,n^0_{t1_z})(k_\beta\hat{q}_3 - k_\alpha\hat{q}_1)] \times [k_\alpha - k_\beta(\hat{k}_3\hat{k}_1 + \hat{q}_3\hat{q}_1)]\,/\,[k_\alpha^2 + k_\beta^2 - 2k_\alpha k_\beta(\hat{k}_3\hat{k}_1 + \hat{q}_3\hat{q}_1)]^{1/2}$,

with $n^0_{t1_z}$ the projection of $\boldsymbol{n_{t1}}$ onto the $\hat{z}$ axis. χ^0_{t1} is the argument of the Fresnel transmission coefficient $t_{\alpha\beta}$, defined in H and V polarizations as, respectively,

$$t^H_{\alpha\beta}\left(\chi^0_{t1}\right) = 1 + r^H_{\alpha\beta}\left(\chi^0_{t1}\right), \tag{9}$$

$$t^V_{\alpha\beta}\left(\chi^0_{t1}\right) = \left[1 - r^V_{\alpha\beta}\left(\chi^0_{t1}\right)\right](\epsilon_{r\alpha}/\epsilon_{r\beta})^{1/2}. \tag{10}$$

The computation of $E_{t,1}$ requires then three-fold integrations. $\hat{k}_{-,1} \in]-\infty;+\infty[$ a priori, but as $E_{t,1}$ is calculated in the far-field zone, evanescent waves can be neglected (which is consistent with the GO approximation). So $\hat{k}_{-,1} \in [-1;+1]$, leading to $\hat{k}_{-,1} = -\sin\theta_{-,1}$. Thus, $d\hat{k}_{-,1}/\hat{q}_{-,1}$ can be reduced to $d\theta_{-,1}$, with $\theta_{-,1} \in [-\pi/2;+\pi/2]$. $x_{A_1}, x_{B_1} \in [-L_0/2;+L_0/2]$ where L_0 is the illuminated surface length.

The field $E_{r,2}$, scattered by the rough layer into the incident medium Ω_1 in the far-field zone, results from the transmission through the surface Σ_A into the medium Ω_2, the reflection onto the surface Σ_B inside Ω_2, and then the transmission through the surface Σ_A back into the medium Ω_3. Taking the illumination functions $\Xi(\boldsymbol{r_{A_1}})$, $\Xi(\boldsymbol{r_{B_1}})$ and $\Xi(\boldsymbol{r_{A_2}})$ into account and using the MSP, it is defined as

$$\begin{aligned} E_{r,2} = -\left(\frac{k_2}{2\pi}\right)^2 \left(\frac{k_1}{2\pi r}\right)^{\frac{1}{2}} E_0 e^{i(k_1 r - \pi/4)} \int \frac{d\hat{k}_{-,1}}{\hat{q}_{-,1}} \frac{d\hat{k}_{+,1}}{\hat{q}_{+,1}} dx_{A_1} dx_{B_1} dx_{A_2} \\ \times \Xi(\boldsymbol{r_{A_1}}) \Xi(\boldsymbol{r_{B_1}}) \Xi(\boldsymbol{r_{A_2}})\, t_{12}\left(\chi^0_{ti}\right) g_{12}\left(\hat{\boldsymbol{k}}_{\boldsymbol{i}}, \hat{\boldsymbol{k}}_{-,\mathbf{1}}, \boldsymbol{n^0_{ti}}\right) \\ \times r_{23}\left(\chi^0_{r-,1}\right) f\left(\hat{\boldsymbol{k}}_{-,\mathbf{1}}, \hat{\boldsymbol{k}}_{+,\mathbf{1}}, \boldsymbol{n^0_{r-,1}}\right) t_{21}\left(\chi^0_{t+,1}\right) g_{21}\left(\hat{\boldsymbol{k}}_{+,\mathbf{1}}, \hat{\boldsymbol{k}}_{\boldsymbol{r}}, \boldsymbol{n^0_{t+,1}}\right) \\ \times e^{ik_1(\hat{\boldsymbol{k}}_{\boldsymbol{i}} \cdot \boldsymbol{r_{A_1}} - \hat{\boldsymbol{k}}_{\boldsymbol{r}} \cdot \boldsymbol{r_{A_2}})}\, e^{ik_2(\hat{\boldsymbol{k}}_{-,\mathbf{1}} \cdot \boldsymbol{r_{A_1B_1}} + \hat{\boldsymbol{k}}_{+,\mathbf{1}} \cdot \boldsymbol{r_{B_1A_2}})}. \end{aligned} \tag{11}$$

The computation of $E_{r,2}$ requires then five-fold integrations. As $E_{r,2}$ is calculated in the far-field zone, evanescent waves can be neglected (which is consistent with the GO approximation), so $d\hat{k}_{-,1}, d\hat{k}_{+,1} \in [-1;+1]$, leading to $\hat{k}_{\pm,1} = \pm\sin\theta_{\pm,1}$. Thus, $d\hat{k}_{\pm,1}/\hat{q}_{\pm,1}$ can be reduced to $d\theta_{\pm,1}$, with $\theta_{\pm,1} \in [-\pi/2;+\pi/2]$. $x_{A_1}, x_{B_1}, x_{A_2} \in [-L_0/2;+L_0/2]$ where L_0 is the illuminated surface length.

Thus, using the same method for the higher orders, that is to say by iterating this 'procedure' for each scattering in reflection or transmission inside the dielectric waveguide, one can obtain the expression of any order of transmitted scattered field $E_{t,n}$ and reflected scattered field $E_{r,n}$ (this is not presented here).

2.3. *Derivation of the scattered fields for a plane lower interface*

When the lower interface Σ_B, separating the media Ω_2 and Ω_3, is assumed to be plane (it is then usually denoted as S_B), the equations can easily be simplified. Indeed, the problem to be solved is the same as the rough case, except that the scattering (in reflection or transmission) from the lower interface is replaced by a simple reflection or transmission, expressed by the corresponding Fresnel coefficient. Thus, in equations (8) and (11), there is no integration over x_{B_1}, and we have: $\Xi(\boldsymbol{r_{B_1}}) = 1$, $\theta_{+,1} = -\theta_{-,1}$, and $\sqrt{\epsilon_{r3}}\sin\theta_t = \sqrt{\epsilon_{r2}}\sin\theta_{-,1}$ (as the lower interface is plane). By neglecting the evanescent waves, this leads to, respectively

$$\begin{aligned} E_{t,1} = \left(\frac{{k_2}^2}{2\pi k_3 r}\right)^{\frac{1}{2}} E_0 e^{i(k_3 r - \pi/4)} \int d\theta_{-,1} dx_{A_1}\, \Xi(\boldsymbol{r_{A_1}})\, \delta\left[\sin\theta_t - \left(\frac{\epsilon_{r2}}{\epsilon_{r3}}\right)^{\frac{1}{2}} \sin\theta_{-,1}\right] \\ \times t_{12}\left(\chi^0_{ti}\right) g_{12}\left(\hat{\boldsymbol{k}}_{\boldsymbol{i}}, \hat{\boldsymbol{k}}_{-,\mathbf{1}}, \boldsymbol{n^0_{ti}}\right) t_{23}(\theta_{-,1})\, e^{ik_1 \hat{\boldsymbol{k}}_{\boldsymbol{i}} \cdot \boldsymbol{r_{A_1}}}\, e^{ik_2 \hat{\boldsymbol{k}}_{-,\mathbf{1}} \cdot \boldsymbol{r_{A_1B_1}}}\, e^{-ik_3 \hat{\boldsymbol{k}}_{\boldsymbol{t}} \cdot \boldsymbol{r_{B_1}}}, \end{aligned} \tag{12}$$

$$E_{r,2} = \frac{k_2}{2\pi}\left(\frac{k_1}{2\pi r}\right)^{\frac{1}{2}} E_0 e^{i(k_1 r - \pi/4)} \int d\theta_{-,1} dx_{A_1} dx_{A_2}\, \Xi(\boldsymbol{r}_{\boldsymbol{A_1}})\Xi(\boldsymbol{r}_{\boldsymbol{A_2}})\delta(\theta_{+,1} + \theta_{-,1})$$
$$\times\, t_{12}\big(\chi^0_{ti}\big) g_{12}\big(\hat{\boldsymbol{k}}_{\boldsymbol{i}}, \hat{\boldsymbol{k}}_{\boldsymbol{-,1}}, \boldsymbol{n}^{\boldsymbol{0}}_{\boldsymbol{ti}}\big)\, r_{23}(\theta_{-,1})\, t_{21}(\chi^0_{t+,1}) g_{21}\big(\hat{\boldsymbol{k}}_{\boldsymbol{+,1}}, \hat{\boldsymbol{k}}_{\boldsymbol{r}}, \boldsymbol{n}^{\boldsymbol{0}}_{\boldsymbol{t+,1}}\big)$$
$$\times\, e^{ik_1(\hat{\boldsymbol{k}}_{\boldsymbol{i}}\cdot \boldsymbol{r}_{\boldsymbol{A_1}} - \hat{\boldsymbol{k}}_{\boldsymbol{r}}\cdot \boldsymbol{r}_{\boldsymbol{A_2}})}\, e^{ik_2(\hat{\boldsymbol{k}}_{\boldsymbol{-,1}}\cdot \boldsymbol{r}_{\boldsymbol{A_1B_1}} + \hat{\boldsymbol{k}}_{\boldsymbol{+,1}}\cdot \boldsymbol{r}_{\boldsymbol{B_1A_2}})}. \tag{13}$$

Thus, in this particular case of a plane lower interface, only two-fold integrations are required for the calculation of $E_{t,1}$ (instead of three), and only three for the calculation of $E_{r,2}$ (instead of five).

3. Incoherent scattering coefficients in the high-frequency limit

The total scattered field $E^{\text{tot}}_{s,n}$ (superscript 'tot' for total; $s \equiv r$ for the reflection case, and $s \equiv t$ for the transmission case) for n-th multiple scattering is $E^{\text{tot}}_{s,n} = \sum_{m=1}^{n} E_{s,m}$. The average scattered power is expressed as

$$\frac{\left\langle \left| E^{\text{tot}}_{s,n} \right|^2 \right\rangle}{2\eta_\alpha} = \sum_{m=1}^{n} \frac{\langle |E_{s,m}|^2 \rangle}{2\eta_\alpha} + \frac{1}{\eta_\alpha}\, \Re e\left(\left\langle \sum_{m=1}^{n-1} E_{s,m} \sum_{p=m+1}^{n} {E_{s,p}}^* \right\rangle \right), \tag{14}$$

with η_α the wave impedance of the considered medium: $\alpha \equiv 1$ for $s \equiv r$ and $\alpha \equiv 2$ for $s \equiv t$. For $n = 2$, we have $E^{\text{tot}}_{s,2} = E_{s,1} + E_{s,2}$, then $\langle |E^{\text{tot}}_{s,2}|^2 \rangle / 2\eta_\alpha = \langle |E_{s,1}|^2 \rangle / 2\eta_\alpha + \langle |E_{s,2}|^2 \rangle / 2\eta_\alpha + \Re e\big(\langle E_{s,1} {E_{s,2}}^* \rangle\big)/\eta_\alpha$, where $\Re e(\ldots)$ is the real part operator, $(\ldots)^*$ the complex conjugate operator, and $\langle \ldots \rangle$ the ensemble average operator. To distinguish the conjugate ${E_{s,n}}^*$ from the field expression $E_{s,n}$, the points $\{A_m, B_m\}$ become $\{A'_m, B'_m\}$, which means that $\{x_{A_m}, x_{B_m}, z_{A_m}, z_{B_m}\} \to \{x_{A'_m}, x_{B'_m}, z_{A'_m}, z_{B'_m}\}$ and $\{\theta_{MM'}\} \to \{\theta'_{MM'}\}$. The incoherent power $P^{\text{tot}}_{s,n}$ is obtained from $P^{\text{tot}}_{s,n} = \langle |E^{\text{tot}}_{s,n}|^2 \rangle / 2\eta_\alpha - |\langle E^{\text{tot}}_{s,n} \rangle|^2 / 2\eta_\alpha$.

To calculate the scattering coefficient of the layer in the high-frequency limit, the geometric optics (GO) approximation ($k_0\sigma_h > 1$, with σ_h being the rms height of the surface) is used for both interfaces. It assumes that the scattering intensity contributes for only closely located correlated points of the surface, M, M', compared to the surface correlation length L_c, such that the coherent contribution $|\langle E^{\text{tot}}_{s,n} \rangle|^2 / 2\eta_\alpha$ can be neglected. Moreover, the height difference $z_{M'} - z_M$ can be expanded as $\gamma_M(x_{M'} - x_M)$, with γ_M the surface slope at the point M. Then, one can express the total scattering coefficient $\sigma^{\text{tot}}_{s,n}$ of a one-dimensional target, defined by [27]

$$\sigma^{\text{tot}}_{s,n}(\theta_i, \theta_s) = \frac{r\ P^{\text{tot}}_{s,n}}{L_0 \cos\theta_i\, p_i}, \qquad \text{with } p_i = \frac{|E_i|^2}{2\eta_1}, \tag{15}$$

where r is the distance of the target, and L_0 the illuminated surface length (L_0 must be greater than the surfaces correlation lengths L_{cA} and L_{cB}). In the above equation, for the specific cases $n = \{1, 2\}$, we have

$$P^{\text{tot}}_{s,1} = p_{s,1} \text{ and } P^{\text{tot}}_{s,2} = p_{s,1} + p_{s,2}, \qquad \text{with} \tag{16}$$

$$\begin{cases} p_{s,1} = \frac{1}{2\eta_\alpha} \langle |E_{s,1}|^2 \rangle \\ p_{s,2} = \frac{1}{2\eta_\alpha} \big[\langle |E_{s,2}|^2 \rangle + 2\, \Re e\big(\langle E_{s,1}\, {E_{s,2}}^* \rangle\big) \big]. \end{cases} \tag{17}$$

In this model, the surface shadowing effects in reflection [22] and in transmission [23] are taken into account. Indeed, for grazing incidence and/or scattering angles, a part of the surface is not seen by the emitter and/or the receiver. This phenomenon has to be taken into account

in order not to over-predict the scattering coefficient. The penumbra effect [28], which occurs for grazing angles, is not taken into account in the model. Then, in theory the shadowing functions used here are not valid for grazing angles; nevertheless, it was shown that in practice they are valid if equation (18) of [28] (Bruce) holds. That is to say, for the typical applications presented here, the geometric shadowing functions can be applied with good approximations up to angles of the order of 85°. Indeed, for the applications presented further (with $\sigma_s = 0.1$ and $\sigma_h \geq \lambda/2$), the numerical application of equation (18) of [28] (Bruce) gives that the validity domain of the GO shadowing function is $\phi_i > 3°$, that is to say $\theta_i < 87°$.

3.1. *Scattering coefficients for a rough lower interface*

3.1.1. First- and second-order reflection scattering coefficients. The calculation of the first-order reflection scattering coefficient $\sigma_{r,1}$, obtained from the statistical correlation of $E_{r,1}$, is relatively simple [23, 29, 30]. It is defined by

$$\sigma_{r,1} = \frac{\left|r_{12}(\chi_{ri}^0)\right|^2}{\cos\theta_i} f^2\left(\hat{\boldsymbol{k}}_{\boldsymbol{i}}, \hat{\boldsymbol{k}}_{\boldsymbol{r}}, \boldsymbol{n}_{\boldsymbol{ri}}^{\boldsymbol{0}}\right) \frac{p_s\left(\gamma_{ri}^0\right)}{|\hat{q}_r - \hat{q}_i|} S_{11}\left(\theta_i, \theta_r | \gamma_{ri}^0\right), \tag{18}$$

with $\gamma_{ri}^0 = -(\hat{k}_r - \hat{k}_i)/(\hat{q}_r - \hat{q}_i)$. $S_{11}(\theta_i, \theta_r | \gamma_{ri}^0)$ is the average bistatic reflection shadowing function expressed by Bourlier *et al*. [22]. One can observe that this scattering coefficient does not depend on the frequency, is independent of the surface height statistics, and can be applied for any given slope statistics.

The second-order contribution is given by $p_{r,2} = p_{r,22} + p_{r,12}$, with $p_{r,22} = \langle |E_{r,2}|^2 \rangle / 2\eta_1$ and $p_{r,12} = \Re e\left(\langle E_{r,1} E_{r,2}{}^* \rangle\right)/\eta_1$. This calculation is much more complicated, as it implies 16-fold integrations (12 random variables: six for the heights and six for the slopes, and four surface variables) for two stationary surfaces (or spatially homogeneous). This number of integrations is too high for a numerical implementation. That is why it is necessary to make further approximations on the model, in order to get a simple mathematical expression of $\sigma_{r,2}$.

First, the stationary phase and the geometric optics approximations are used for both interfaces, at each scattering point. In the high-frequency limit, it is possible to demonstrate that the term $p_{r,12} = 0$ owing to the shadow. Furthermore, to be consistent with the GO approximation, the evanescent waves must be neglected, and it is necessary to suppose that the wavenumber inside the intermediate medium k_2 is real. Let us notice that the latter restrictive hypothesis implies that the model itself cannot handle lossy dielectric media, yet, we will show later that it is possible to consider it properly. Moreover, the former hypothesis does not mean that the scattering points are in far field from one another. This principle is the same as the one used for the double scattering from a single interface: the authors neglect the evanescent waves [20, 21, 31].

Using the same approach as for the double scattering from a single rough interface [20, 21, 19], one can divide this problem into coincidental and anti-coincidental cases. The coincidental case corresponds to A_1' close to A_1, B_1' close to B_1, and A_2' close to A_2 (compared to the surface correlation lengths L_{cA} and L_{cB}). This case contributes for all scattering angles. The anti-coincidental case corresponds to A_1' close to A_2, B_1' close to B_1, and A_2' close to A_1 (compared to the surface correlation lengths L_{cA} and L_{cB}). This case may contribute only for scattering angles in and around the backscattering direction. For the coincidental case, the points of successive reflections A_1, B_1, A_2 can be considered as uncorrelated between one another, which simplifies the final equation.

By contrast, for the anti-coincidental case, to quantify the backscattering enhancement properly, one has to take the correlations between the points of successive reflections into account. Then, this complicates the problem to be solved a lot, implying an additional numerical

integration by considering Gaussian statistics. After tedious calculations, one obtains for the anti-coincidental contribution $\sigma_{r,2a}$

$$\sigma_{r,2a} = \frac{k_1}{2\pi\cos\theta_i}\ 2\Re e\Bigg(\int_{-\frac{\pi}{2}}^{+\frac{\pi}{2}}\int_{-\frac{\pi}{2}}^{0} d\theta_{-,1}d\theta'_{-,1}\ \frac{t_{12}(\chi_{ti}^0)t_{12}^*(\chi_{ti}^{0\prime})}{\left|\frac{(\hat{q}_{-,1}+\hat{q}'_{-,1})}{2}-\frac{k_1}{k_2}\frac{(\hat{q}_i-\hat{q}_r)}{2}\right|^2}$$
$$\times\, g_{12}(\hat{\boldsymbol{k}}_{\boldsymbol{i}},\hat{\boldsymbol{k}}_{-,\mathbf{1}},\boldsymbol{n}_{\boldsymbol{tc1}}^{\mathbf{0}})g_{12}(\hat{\boldsymbol{k}}_{\boldsymbol{i}},\hat{\boldsymbol{k}}'_{-,\mathbf{1}},\boldsymbol{n}_{\boldsymbol{tc2}}^{\mathbf{0}})r_{23}(\theta_{-,1})r_{23}^*(\theta'_{-,1})t_{21}(\chi_{t+,1}^0)t_{21}^*(\chi_{t+,1}^{0\prime})$$
$$\times\, g_{21}(\hat{\boldsymbol{k}}_{+,\mathbf{1}},\hat{\boldsymbol{k}}_{\boldsymbol{r}},\boldsymbol{n}_{\boldsymbol{tc2}}^{\mathbf{0}})g_{21}(\hat{\boldsymbol{k}}'_{+,\mathbf{1}},\hat{\boldsymbol{k}}_{\boldsymbol{r}},\boldsymbol{n}_{\boldsymbol{tc1}}^{\mathbf{0}})\ S_{1221}(\hat{\boldsymbol{k}}_{\boldsymbol{i}},\hat{\boldsymbol{k}}_{-,\mathbf{1}},\hat{\boldsymbol{k}}'_{-,\mathbf{1}},\hat{\boldsymbol{k}}_{\boldsymbol{r}}|\gamma_{tc1}^0,\gamma_{tc2}^0)$$
$$\times\, e^{-2ik_2(\hat{q}_{-,1}-\hat{q}'_{-,1})\bar{H}}\int_{x^{\min}}^{x^{\max}} dx_{mc}\, e^{i(k_i+k_r-k_{-,1}-k'_{-,1})x_{mc}}\ I_1\Bigg) \tag{19}$$

where $x_{mc} = x_{c1} - x_{c2}$ with $x_{c1} = (x_{A_1} + x_{A'_2})/2$, $x_{c2} = (x_{A_2} + x_{A'_1})/2$, and $x_{mc} \in [x^{\min}; x^{\max}]$. $q_1 = q_i + q_r - q_{-,1} + q'_{-,1}$, $q_2 = -q_i - q_r - q_{-,1} + q'_{-,1}$, $\boldsymbol{n}_{\boldsymbol{tc1}}^{\mathbf{0}} = -\gamma_{tc1}^0\hat{\boldsymbol{x}} + \hat{\boldsymbol{z}}$ with $\gamma_{tc1}^0 = -\frac{(k_i-k_r)-(k_{-,1}-k'_{-,1})}{(q_i-q_r)-(q_{-,1}+q'_{-,1})}$, and $\boldsymbol{n}_{\boldsymbol{tc2}}^{\mathbf{0}} = -\gamma_{tc2}^0\hat{\boldsymbol{x}} + \hat{\boldsymbol{z}}$ with $\gamma_{tc2}^0 = -\frac{(k_i-k_r)+(k_{-,1}-k'_{-,1})}{(q_i-q_r)-(q_{-,1}+q'_{-,1})}$. I_1 represents the statistical averaging of $e^{iq_1z_{c1}}e^{iq_2z_{c2}}$ over z_{c1} and z_{c2} (also called the characteristic function of z_{c1} and z_{c2}). For Gaussian slope statistics, after tedious calculations, one can express I_1 as

$$I_1 \equiv I_1(x_{mc}) = p_s(\gamma_{tc1}^0, \gamma_{tc2}^0; x_{mc})\ f(q_1, q_2, \gamma_{tc1}^0, \gamma_{tc2}^0; x_{mc}), \tag{20}$$

with

$$p_s(\gamma_{tc1}^0, \gamma_{tc2}^0) = \frac{1}{2\pi\sqrt{\sigma_s^4 - W_2^2}}\exp\left[-\frac{(\sigma_s^2{\gamma_{tc1}^0}^2 + \sigma_s^2{\gamma_{tc2}^0}^2 + 2W_2\gamma_{tc1}^0\gamma_{tc2}^0)}{2(\sigma_s^4 - W_2^2)}\right] \tag{21}$$

and

$$f(q_1, q_2, \gamma_{tc1}^0, \gamma_{tc2}^0) = e^{i\frac{W_1}{(\sigma_s^4-W_2^2)}[(q_1\sigma_s^2-q_2W_2)\gamma_{tc2}^0-(q_2\sigma_s^2-q_1W_2)\gamma_{tc1}^0]}$$
$$\times\, e^{-\frac{1}{2(\sigma_s^4-W_2^2)}[2q_1q_2(W_0\sigma_s^4+W_1W_2-W_0W_2^2)-(q_1^2+q_2^2)W_1^2\sigma_s^2]}$$
$$\times\, e^{-\frac{1}{2}(q_1^2+q_2^2)\sigma_h^2}, \tag{22}$$

with W_0 the autocorrelation function between z_{c1} and z_{c2} (which is a function of the horizontal distance x_{mc}), W_1 its first derivative, and W_2 its second derivative. I_1 in (20) is a function of x_{mc}, as p_s and f implicitly depend on x_{mc} through W_0, W_1, and W_2. When the slopes are uncorrelated, $W_0 = 0$, $W_1 = 0$, $W_2 = 0$, leading to the uncorrelated formula $I_1 = p_s(\gamma_{tc1}^0)p_s(\gamma_{tc2}^0)\exp[-1/2(q_1^2 + q_2^2)\sigma_h^2]$. The main difficulty is then to determine or at least to evaluate the minimum and maximum values of x_{mc}, $x^{\min}$ and $x^{\max}$, which are random variables depending on the heights and the slopes of these points. For typical applications presented here (that is to say for slight surface slopes and moderate mean layer thicknesses in the high-frequency limit) the numerical results of $\sigma_{r,2a}$ showed that can be neglected. This is in agreement with results from the literature [32, 33], which showed that for the scattering from a rough layer, where the lower interface is plane, this case contributes only when the mean layer thickness $\bar{H}$ satisfies the condition

$$\bar{H} > \frac{\sqrt{\epsilon_{r2}}}{\sqrt{\epsilon_{r2}-1}}R_{cA}, \tag{23}$$

with R_{cA} the radius of curvature of the upper rough surface. For the simulations presented here, $\bar{H}$ is much smaller than R_{cA}: this confirms that the anti-coincidental case does not contribute

for the typical applications presented here. Therefore, this case will not be considered further for the sake of simplicity.

Thus, neglecting the anti-coincidental contribution, one can obtain a simple expression of the second-order scattering coefficient $\sigma_{r,2}$, defined by

$$\begin{aligned}\sigma_{r,2} = {} & \frac{1}{\cos\theta_i}\int_{-\frac{\pi}{2}}^{+\frac{\pi}{2}}\int_{-\frac{\pi}{2}}^{+\frac{\pi}{2}} d\theta_{-,1}\, d\theta_{+,1} \\ & \times \left|t_{12}\left(\chi^0_{ti}\right) g_{12}\left(\hat{\boldsymbol{k}}_{\boldsymbol{i}}, \hat{\boldsymbol{k}}_{\boldsymbol{-,1}}, \boldsymbol{n}^{\boldsymbol{0}}_{\boldsymbol{ti}}\right)\right|^2 \frac{p_s\left(\gamma^0_{tA_1}\right)}{\left|\hat{q}_{-,1} - \frac{k_1}{k_2}\hat{q}_i\right|} S_{12}\left(\theta_i, \theta_{-,1}|\gamma^0_{tA_1}\right) \\ & \times \left|r_{23}\left(\chi^0_{r-,1}\right) f\left(\hat{\boldsymbol{k}}_{\boldsymbol{-,1}}, \hat{\boldsymbol{k}}_{\boldsymbol{+,1}}, \boldsymbol{n}^{\boldsymbol{0}}_{\boldsymbol{r-,1}}\right)\right|^2 \frac{p_s(\gamma^0_{rB_1})}{|\hat{q}_{+,1} - \hat{q}_{-,1}|} S_{22}\left(\theta_{-,1}, \theta_{+,1}|\gamma^0_{rB_1}\right) \\ & \times \left|t_{21}\left(\chi^0_{t+,1}\right) g_{21}\left(\hat{\boldsymbol{k}}_{\boldsymbol{+,1}}, \hat{\boldsymbol{k}}_{\boldsymbol{r}}, \boldsymbol{n}^{\boldsymbol{0}}_{\boldsymbol{t+,1}}\right)\right|^2 \frac{p_s(\gamma^0_{tA_2})}{\left|\hat{q}_r - \frac{k_2}{k_1}\hat{q}_{+,1}\right|} S_{21}\left(\theta_{+,1}, \theta_r|\gamma^0_{tA_2}\right). \end{aligned} \tag{24}$$

To obtain physical results for grazing angles for the case with shadow, the configurations of $\theta_{+,1}$ and θ_r that induce local scattering angles greater than $\pi/2$ in absolute values must be omitted. The slopes $\gamma^0_{tA_1}, \gamma^0_{rB_1}, \gamma^0_{tA_2}$ are defined by

$$\gamma^0_{tA_1} = -(k_2\hat{k}_{-,1} - k_1\hat{k}_i)/(k_2\hat{q}_{-,1} - k_1\hat{q}_i), \tag{25}$$

$$\gamma^0_{rB_1} = -(\hat{k}_{+,1} - \hat{k}_{-,1})/(\hat{q}_{+,1} - \hat{q}_{-,1}), \tag{26}$$

$$\gamma^0_{tA_2} = -(k_1\hat{k}_r - k_2\hat{k}_{+,1})/(k_1\hat{q}_r - k_2\hat{q}_{+,1}). \tag{27}$$

$S_{12}(\theta_i, \theta_{-,1}|\gamma^0_{tA_1})$, $S_{22}(\theta_{-,1}, \theta_{+,1}|\gamma^0_{rB_1})$, $S_{21}(\theta_{+,1}, \theta_r|\gamma^0_{tA_2})$ are the bistatic shadowing functions, in transmission from the medium Ω_1 into the medium Ω_2, in reflection inside the medium Ω_2 and onto the medium Ω_3, and in transmission from the medium Ω_2 back into the medium Ω_1, respectively. One can show, for *any* random process, that [34, 23]:

$$S_{12}\left(\theta_i, \theta_{-,1}|\gamma^0_{tA_1}\right) = B(1 + \Lambda(\mu_i), 1 + \Lambda(\mu_{-,1})), \tag{28}$$

$$S_{21}\left(\theta_{+,1}, \theta_r|\gamma^0_{tA_2}\right) = B(1 + \Lambda(\mu_{+,1}), 1 + \Lambda(\mu_r)), \tag{29}$$

where B is the beta function (also called the Eulerian integral of the first kind), Λ is the function defined by $\Lambda(\mu) = 1/\mu \int_\mu^{+\infty}(\gamma - \mu)\, p_s(\gamma)\, d\gamma$, with $\mu = |\cot\theta|$ the absolute slope of the considered angle.

Thus, the problem can be reduced to only two-fold integrations, which enables a fast numerical implementation. One can observe that expression (24) under the geometric optics approximation can be applied for any given slope statistics, and is independent of the frequency (within the domain of validity of the model). Moreover, assuming that the points of successive reflections A_1, B_1 and A_2 are uncorrelated, this expression appears as the product of three elementary scattering coefficients of single interfaces, each one corresponding to each scattering in reflection or transmission inside the rough dielectric waveguide. Indeed, the first one corresponds to the scattering in transmission from the point A_1 of Σ_A into the medium Ω_2, the second one to the scattering in reflection from the point B_1 of Σ_B inside Ω_2, and the third one to the scattering in transmission from the point A_2 of Σ_A back into the medium Ω_1. The two-fold integrals account for the energy scattered by the rough surfaces in all scattering directions.

Then, under the GO approximation, to obtain the total scattering coefficient $\sigma^{\text{tot}}_{r,2}$, the single $\sigma_{r,1}$ and double $\sigma_{r,2}$ contributions are incoherently added.

3.1.2. First-order transmission scattering coefficient. Using exactly the same approach as for $\sigma_{r,1}$ and $\sigma_{r,2}$, one can obtain the expression of the first-order transmission scattering coefficient $\sigma_{t,1}$. Thus, $\sigma_{t,1}$ is defined by

$$\begin{aligned}\sigma_{t,1} = \sqrt{\frac{\epsilon_{r3}}{\epsilon_{r1}}}\,\frac{1}{\cos\theta_i}\int_{-\frac{\pi}{2}}^{+\frac{\pi}{2}} d\theta_{-,1} \\ \times \left|t_{12}\left(\chi_{ti}^0\right) g_{12}\left(\hat{\boldsymbol{k}}_{\boldsymbol{i}}, \hat{\boldsymbol{k}}_{-,\mathbf{1}}, \boldsymbol{n}_{\boldsymbol{ti}}^{\mathbf{0}}\right)\right|^2 \frac{p_s\left(\gamma_{tA_1}^0\right)}{\left|\hat{q}_{-,1} - \frac{k_1}{k_2}\hat{q}_i\right|} S_{12}\left(\theta_i, \theta_{-,1}|\gamma_{tA_1}^0\right) \\ \times \left|t_{23}\left(\chi_{t-,1}^0\right) g_{23}\left(\hat{\boldsymbol{k}}_{-,\mathbf{1}}, \hat{\boldsymbol{k}}_{\boldsymbol{t}}, \boldsymbol{n}_{\boldsymbol{t}-,\mathbf{1}}^{\mathbf{0}}\right)\right|^2 \frac{p_s(\gamma_{tB_1}^0)}{\left|\hat{q}_t - \frac{k_2}{k_3}\hat{q}_{-,1}\right|} S_{23}\left(\theta_{-,1}, \theta_t|\gamma_{tB_1}^0\right), \qquad (30)\end{aligned}$$

with $\gamma_{tB_1}^0 = -(k_3\hat{k}_t - k_2\hat{k}_{-,1})/(k_3\hat{q}_t - \hat{k}_2 q_{-,1})$, and $S_{23}(\theta_{-,1}, \theta_t|\gamma_{tB_1}^0) = B\left[1 + \Lambda(\mu_{-,1}), 1 + \Lambda(\mu_t)\right]$. The same concluding remarks on the expression of $\sigma_{t,1}$ can be made as for $\sigma_{r,2}$.

3.2. *Scattering coefficients for a plane lower interface*

For the case of a plane lower interface, the expressions of the scattering coefficients are similar and much simpler, as the general term $\int_{-\frac{\pi}{2}}^{+\frac{\pi}{2}} d\theta_{+,m}\, s_{r,23}^{B_m}$ is replaced by $|r_{23}(\theta_{-,m})|^2\,\delta(\theta_{+,m} - \theta_{-,m})$, and the general term $s_{t,23}^{B_m}$ is replaced by $|t_{23}(\theta_{-,n})|^2\,\delta[\sin\theta_t - (\frac{\epsilon_{r2}}{\epsilon_{r3}})^{\frac{1}{2}}\sin\theta_{-,n}]$. For $m = 1$, $s_{r,23}^{B_1} = |r_{23}(\chi_{r-,1}^0)\, f(\hat{\boldsymbol{k}}_{-,\mathbf{1}}, \hat{\boldsymbol{k}}_{+,\mathbf{1}}, \boldsymbol{n}_{\boldsymbol{r}-,\mathbf{1}}^{\mathbf{0}})|^2 \frac{p_s(\gamma_{rB_1}^0)}{|\hat{q}_{+,1} - \hat{q}_{-,1}|} S_{22}(\theta_{-,1}, \theta_{+,1}|\gamma_{rB_1}^0)$ and $s_{t,23}^{B_1} = |t_{23}(\chi_{t-,1}^0)\, g_{23}(\hat{\boldsymbol{k}}_{-,\mathbf{1}}, \hat{\boldsymbol{k}}_{\boldsymbol{t}}, \boldsymbol{n}_{\boldsymbol{t}-,\mathbf{1}}^{\mathbf{0}})|^2 \frac{p_s(\gamma_{tB_1}^0)}{|\hat{q}_t - \frac{k_2}{k_3}\hat{q}_{-,1}|} S_{23}(\theta_{-,1}, \theta_t|\gamma_{tB_1}^0)$. For this simpler case, $\sigma_{r,2}$ is calculated with only one numerical integration, allowing us to obtain results quasi-instantaneously.

4. Numerical results

For the simulations, the considered system is a layer of permittivity ϵ_{r2}, with mean layer thickness $\bar{H} = 6\lambda$, overlying a perfectly conducting medium of permittivity $\epsilon_{r3} = i\infty$. We choose to take a lower medium as being perfectly conducting, so that the contribution of the second-order scattering coefficient $\sigma_{r,2}$ is the highest. The surface rms height of each interface equals half the incident electromagnetic wavelength, $\sigma_h = \lambda_0/2$, and the surface rms slope is taken to be $\sigma_s = 0.1$. This corresponds to the validity domain of the model. The two random rough surfaces are assumed to be stationary, and we will consider Gaussian slope statistics for the simulations. Only the first reflection inside the layer is considered, and its contribution is compared to the scattering from the upper interface. That is to say, one will study the comparison between the second-order total reflection scattering coefficient $\sigma_{r,2}^{\text{tot}} = \sigma_{r,1} + \sigma_{r,2}$ and the first-order one $\sigma_{r,1}^{\text{tot}} = \sigma_{r,1}$. Simulations are presented for $\theta_i = 0^\circ$ and $\theta_i = -20^\circ$.

Computer simulations for optics applications, with bistatic configuration, are presented to validate the model, by comparison with a benchmark numerical method [24, 25] based on the method of moments. The simulation parameters of this method used for each surface are the surface length $L = 150\lambda$, the number of sampling points of the surface $n_i = 1500$, the number of realizations of the surface $N = 50$, and the attenuation parameter of the incident Thorsos beam $g = L/10$. A comparison between a rough and a plane lower interfaces is made, and the case of a lossy inner medium Ω_2 is studied.

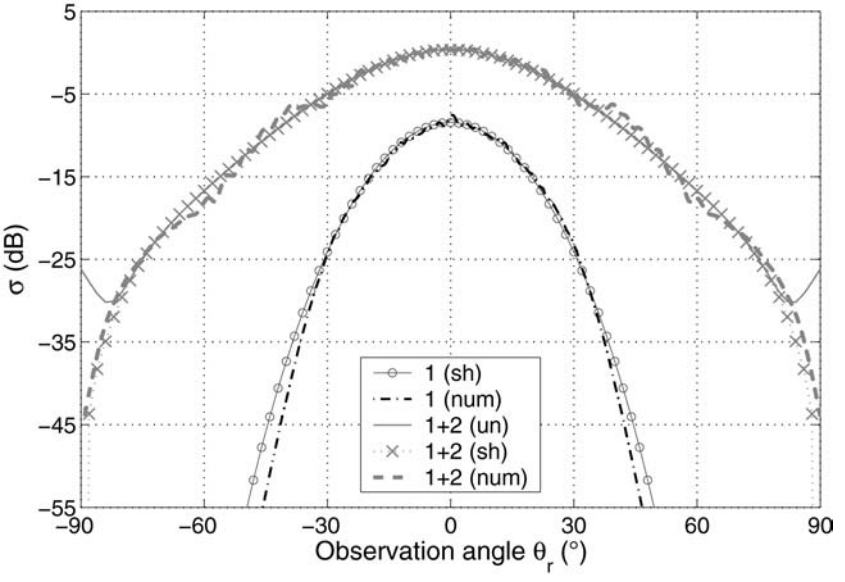

Figure 2. Simulations of the contributions of the first- and second-order scattering coefficients, $\sigma_{r,1}$ and $\sigma_{r,2}$ in dB, versus the reflection scattering angle θ_r (in $^\circ$) for V polarization, for $\epsilon_{r2} = 3$ and $\epsilon_{r3} = i\infty$, and for $\theta_i = 0^\circ$. For the first-order contribution, comparison of the model with shadow (circled line) with the reference numerical method (dashdot line). For the second-order contribution, comparison of the model without shadow (full line) and the model with shadow (crossed dotted line) with the reference numerical method (dashed line).

5. Model validation by comparison with a benchmark numerical method

To validate the results, an exact reference method is needed. A rigorous way to model the scattering from rough interfaces is done numerically by means of integral methods [30], where the fields and their normal derivative on both interfaces are unknowns. These unknowns are sampled by applying a method of moments [35]; the bulk of the work is then to invert the corresponding linear system. Nevertheless, for the case of two rough interfaces, this implies a large number of unknowns. Then, a direct inversion (LU) is inappropriate. Thus, one uses here an original numerical method, the recent Propagation-inside-Layer Expansion (PILE) method [24, 25], in order to deal with this kind of problems on a standard office computer.

The studied model is compared to the PILE method, for $\theta_i = \{0^\circ, -20^\circ\}$, for the optics domain application. The configuration is bistatic, where the scattering angle θ_r lies in $[-90^\circ; +90^\circ]$. Simulations of the contributions of the first- and second-order bistatic reflection scattering coefficients, $\sigma_{r,1}$ and $\sigma_{r,2}$ (that is to say, the total scattering coefficients $\sigma_{r,1}^{\text{tot}}$ and $\sigma_{r,2}^{\text{tot}}$), are presented for $\theta_i = 0^\circ$ in figure 2, and for $\theta_i = -20^\circ$ in figure 3.

In both figures, for the first-order contribution $\sigma_{r,1}$, a comparison is made between the model with shadow, plotted as the circled line, and the PILE method, plotted as the dashdot line. The numerical results highlight good agreement of the model with the reference method, in both V and H polarizations (only the V polarization is represented here), and for both incidence angles, around the specular direction $\theta_r = -\theta_i$. The model without shadow is not represented here as for this configuration, there is no difference with the model with shadow: indeed, for slight slopes and moderate incidence angles, the surface is shadowed only for very high grazing scattering angles, which have no effect on $\sigma_{r,1}$ in this case.

For the contribution of the second-order scattering coefficient $\sigma_{r,2}$ (that is to say the total second-order scattering coefficient $\sigma_{r,2}^{\text{tot}}$), a comparison is made between the model, plotted as the full line for the model without shadow and in crossed dotted line for the model with shadow,

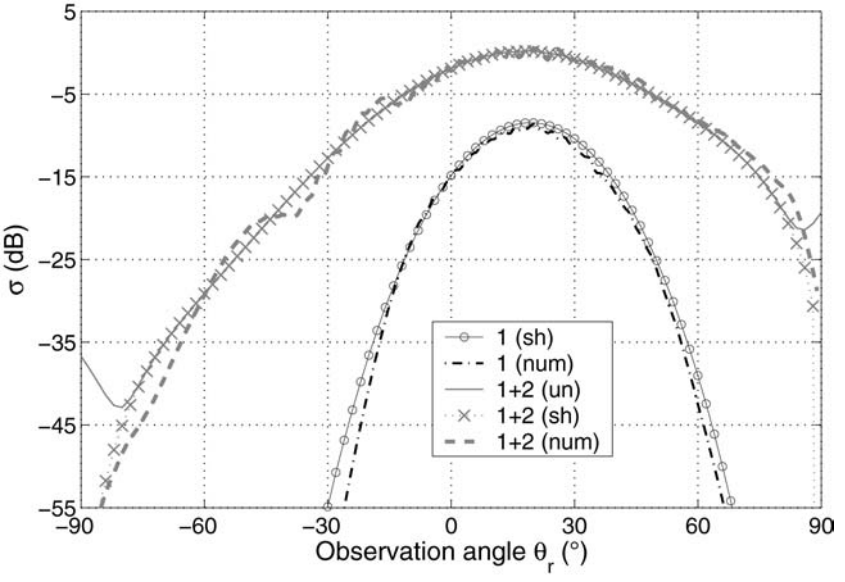

Figure 3. Same simulations as figure 2, but with $\theta_i = -20^\circ$.

and the PILE method, plotted as the dashed line. First, one can observe that this contribution is significant, not only in and around the specular direction, but in all reflection scattering directions. Indeed, as the permittivity of the inner medium is close to that of the upper medium, the major part of the incident energy is transmitted into the inner medium towards the perfectly conducting lower interface. Then, all this energy is scattered in reflection towards the upper interface, which in major part is transmitted back into the incident medium. Thus, the second-order scattering coefficient has a significant contribution to the total scattering coefficient by comparison with the first-order. Second, the scattered intensity is not concentrated around the specular direction, contrary to the first-order, but more widely spread around all scattering angles. Indeed, the second-order scattered power underwent three successive scatterings: two scatterings in transmission, which are less significant than the scattering in reflection by the lower interface. The numerical results also highlight good agreement of the model with the reference numerical (PILE) method, in both V and H polarizations (only the V polarization is represented here), and for both incidence angles. The results confirm that for this configuration, the shadowing effect contributes only for grazing scattering angles (over 75–80° here), but is of importance for these angles to get physical numerical results, and consistent with the numerical method. For both incidence angles, the differences between the studied model and the PILE method are due to the difficulties in defining the simulation parameters of the fast numerical method, which have a significant influence on the scattering coefficient. The numerical method needs a great number of samples of the surface to be accurate, which is very extensive in computing time and memory space compared to the GO approximation. In addition, the configurations where the scattering coefficient of the GO approximation are higher than the numerical method cannot be attributed to the multiple scattering on the same interface. Indeed, when double scattering phenomena from a single interface occurs, there is an increase in scattering (and not a decrease) since the GO approximation is an incoherent approach. As a result, a decrease of the scattering coefficient (from the GO approximation to the numerical method) at low grazing angles cannot be attributed to multiple scattering on the same interface. Moreover, for typical cases presented here (i.e. surfaces with rms slope

$\sigma_s = 0.1$, bistatic configuration, and $\theta_i \leq 20^\circ$), it is well known [36, 37] that multiple scattering phenomena can be neglected.

Thus, the model with shadow is in good agreement with the reference numerical method. One can find applications in advanced remote sensing, where the emitter and the receiver are in different places, like for the remote sensing of sand over granite [38], ocean ice [39, 40] (when the ice layer can be supposed as homogeneous), and oil slicks on the ocean. One may also find applications to optical tomography of biological media [41, 42], as a basic fast model when the media can be supposed as homogeneous.

6. Comparison between a rough and a plane lower interface

This section is devoted to the comparison of the model between the case of a rough lower interface and a plane lower interface, and their influence on the contribution of the second-order scattering coefficient $\sigma_{r,2}$.

Simulations are presented in the bistatic configuration $\theta_r \in [-90^\circ; +90^\circ]$, for $\theta_i = 0^\circ$ in figure 4 and $\theta_i = -20^\circ$ in figure 5. The first-order contribution $\sigma_{r,1}$ is plotted as the circled line for comparison. The second-order contribution $\sigma_{r,2}$ for a rough lower interface is plotted as the crossed dotted line, and the one for a plane lower interface is plotted as the dashed line. The typical CPU time to calculate $\sigma_{r,1}$ and $\sigma_{r,2}$ for the case of a plane lower interface is about 34 ms for given θ_i and θ_r, with 40 sampling points of $\theta_{-,1}$ for the numerical integration (in comparison with 190 ms for a rough lower interface).

For $\theta_i = 0^\circ$, the difference on the second-order contribution $\sigma_{r,2}$ between a rough and a plane lower interface is clear. For a plane lower interface, the second-order contribution is concentrated around the specular direction $\theta_r = -\theta_i$. Indeed, as the lower interface is plane, the energy incident on the lower interface is not scattered in all directions like for the rough case but reflected in the specular direction. On the contrary, for a rough lower interface, the

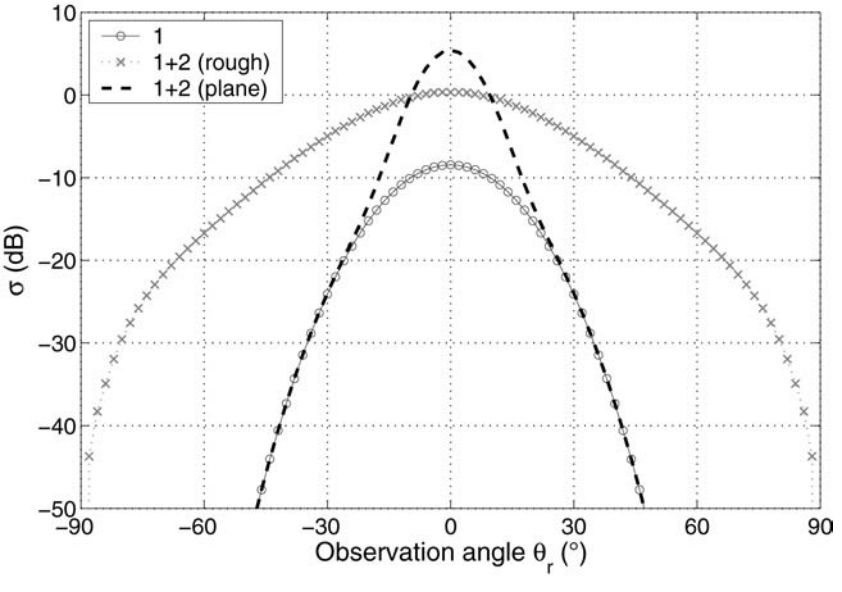

Figure 4. Simulations of the contribution of the second-order scattering coefficient, $\sigma_{r,2}$ in dB, versus the reflection scattering angle θ_r (in $^\circ$) for V polarization, for $\epsilon_{r2} = 3$ and $\epsilon_{r3} = i\infty$, and for $\theta_i = 0^\circ$: comparison of the case of a rough lower interface (crossed dotted line) with the case of a plane lower interface (dashed line). The first-order contribution is also plotted (circled line) for comparison.

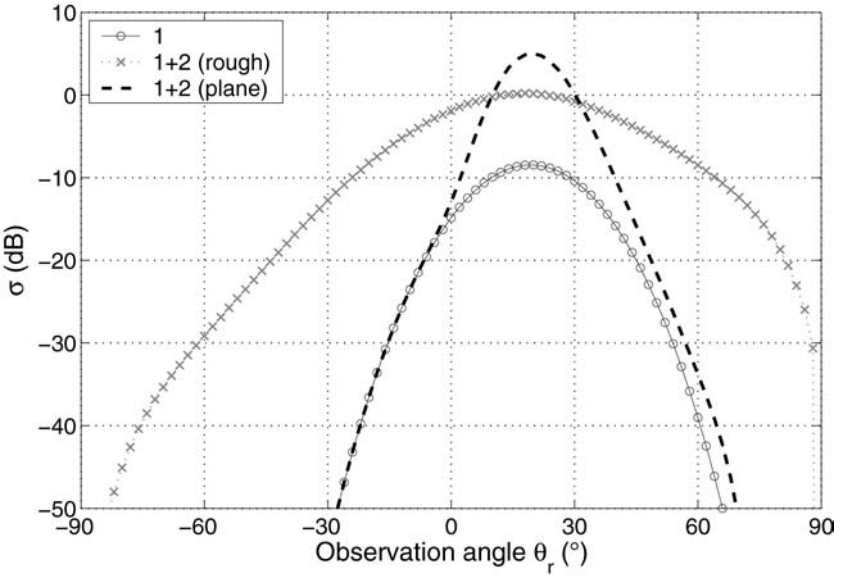

Figure 5. Same simulations as figure 4, but with $\theta_i = -20^\circ$.

second-order contribution is lower in and around the specular direction, and is more uniformly distributed in all scattering angles. Indeed, the rough lower interface scatters energy in all directions. This significant difference in the spread of the scattered energy confirms that the scattering in reflection is much more significant than the two scatterings in transmission. The same observation can be made for $\theta_i = -20^\circ$. Then, it is easy to discriminate such a system with a rough lower interface from the one with a plane lower interface. One can find applications to the characterization of optical materials, where one interface of the glass is rough, and the other one is smooth [43–47], for cases where the surface roughness is larger than, or at least of the order of, half the electromagnetic wavelength.

7. Study of a lossy inner medium

One can notice that the expressions of the scattering coefficients are independent of the layer mean thickness $\bar{H}$ (neglecting the anti-coincidental case), which means that the model itself cannot determine a layer thickness. This corresponds to the use of the GO approximation, in which the phase term is not taken into account. Thus, the model itself cannot deal with lossy inner media (Ω_2, with $\epsilon_{r2} \equiv \underline{\epsilon}_{r2} \in \mathbb{C}\backslash\mathbb{R}$). Still, we will see in this section that it is easy to take this case into account: using minor adjustments to the model, one has a good estimate of the scattering coefficients of the lossy layer.

7.1. *Theoretical analysis of losses from a lossy dielectric inner medium*

For the first-order scattering coefficient $\sigma_{r,1}$, the only modification is that the Fresnel reflection coefficient r_{12} becomes complex owing to $\underline{\epsilon}_{r2}$. Then, in equation (18), in $|r_{12}(\chi^0_{ri})|^2$, $|\ldots|$ does not represent an absolute value any more, but a modulus. By contrast, for the second-order scattering coefficient $\sigma_{r,2}$, there are several minor modifications.

First, there is a problem in defining the *physical* propagation angles inside the lossy inner medium Ω_2, $\theta_{-,1}$ and $\theta_{+,1}$. Indeed, with lossless media, the latter are usually obtained using the refraction and reflection Snell–Descartes laws

$$\sqrt{\epsilon_{r2}}\sin\chi_t = \sqrt{\epsilon_{r1}}\sin\chi_i, \tag{31}$$

$$\chi_r = -\chi_i, \tag{32}$$

with χ_i the local incidence angle, χ_t the local transmission angle, and χ_r the local reflection angle from the local normal to the considered surface. Then, with the knowledge of the local surface slope and the incidence angle θ_i, one can easily obtain $\theta_{-,1}$ with the use of the refraction Snell–Descartes law (31) at the upper interface, and then $\theta_{+,1}$ with the use of the reflection Snell–Descartes law (32) at the lower interface. The trouble is, with $\epsilon_{r2} \equiv \underline{\epsilon}_{r2} \in \mathbb{C}$, as the term of the right hand-side of equation (31) is real, the product $\sqrt{\underline{\epsilon}_{r2}}\sin\underline{\chi}_t$ of the left hand-side of equation (31) must be real, which implies that $\underline{\chi}_t$ is complex (as $\underline{\epsilon}_{r2}$ is complex). However, we need to determine the *physical* (with then a real value) local propagation angle χ_t^{phys} inside Ω_2 (so as to determine $\theta_{-,1}$ with the knowledge of the local surface slope), which is not simply the real part of $\underline{\chi}_t$. It is given by [48, 49]

$$\tan\chi_t^{\text{phys}} = \frac{\sin\chi_i}{p}, \quad \text{with} \tag{33}$$

$$p = \frac{1}{\sqrt{2}}\Big[\sqrt{\left(\epsilon'_{r2} - \sin^2\chi_i\right)^2 + \epsilon''^{\,2}_{r2}} + \left(\epsilon'_{r2} - \sin^2\chi_i\right)\Big]^{\frac{1}{2}}, \tag{34}$$

where $\underline{\epsilon}_{r2} = \epsilon'_{r2} + i\,\epsilon''_{r2}$, and $p = \Re e(\sqrt{\underline{\epsilon}_{r2} - \sin^2\underline{\chi}_t})$. Then, this allows one to determine $\theta_{-,1}$, and then $\theta_{+,1}$ using equation (32) on the lower surface, with the knowledge of the local surface slope.

Second, in equation (24), the reflection and transmission Fresnel coefficients become complex, and $|\ldots|$ represents a modulus, and not an absolute value any more. Let us note that the Fresnel reflection coefficient $r_{23}(\chi^0_{r-,1})$, and the Fresnel transmission coefficient $t_{21}(\chi^0_{t+,1})$ use local incidence angles, $\chi^0_{r-,1}$ and $\chi^0_{t+,1}$, that are defined with the *physical* angles $\theta_{-,1}$ and $\theta_{+,1}$, respectively, and the local slope of the surface considered.

Third, with the knowledge of the physical propagation angles $\theta_{-,1}$ and $\theta_{+,1}$ inside Ω_2, the mean layer thickness $\bar{H}$, and the slope probability density function (PDF) of the two surfaces, one can determine the field path from the point A_1 to the point B_1, and from the point B_1 to the point A_2. Thus, it is possible to determine the propagation loss $\mathcal{A}$ of the power inside the lossy inner medium Ω_2 (from A_1 to B_1, and from B_1 to A_2).

7.2. *Estimation of the losses for numerical implementation*

In order to numerically implement the model for the specific case of a lossy inner medium Ω_2 in a fast and easy way, minor changes to the initial model can be made.

First, to evaluate the propagation loss $\mathcal{A}$, we will only consider here the simple case of plane interfaces (indeed, even if the rough case can be calculated, considering only the plane case will be satisfactory). Then, the propagation loss can easily be evaluated with the knowledge of θ_i, $\theta_{-,1}$, and $\overline{H}$. Then, this power propagation loss $\mathcal{A}$ is evaluated for plane interfaces by the expression $\mathcal{A}_{pl}$ (called the planar power propagation loss) as

$$\mathcal{A} \simeq \mathcal{A}_{pl} = \exp\big(-4k_0\overline{H}q\,/\cos\theta_t^{\text{plane}}\big), \quad \text{with} \tag{35}$$

$$q = \frac{1}{\sqrt{2}}\left[\sqrt{\left(\epsilon'_{r2} - \sin^2\theta_i\right)^2 + \epsilon''^{\,2}_{r2}} - \left(\epsilon'_{r2} - \sin^2\theta_i\right)\right]^{\frac{1}{2}}, \tag{36}$$

where θ_t^{plane} is defined by the refraction Snell–Descartes law (31) at the upper interface, for the case of a plane interface where the local incidence angle χ_i equals θ_i, and $q = \Im m(\sqrt{\underline{\epsilon}_{r2} - \sin^2 \underline{\chi}_t})$. Then, the physical local refraction angle χ_t^{phys} equals $\theta_{-,1} \equiv \theta_t^{\text{plane}}$ (as the lower interface is also plane, one also obtains $\theta_{+,1} = -\theta_t^{\text{plane}}$).

Second, although $\theta_{-,1}$ and $\theta_{+,1}$ can be calculated rigorously, it can be interesting to evaluate them with few modifications to the initial model. Then, one can use the following approximation: in the refraction Snell–Descartes law (31), instead of using the complex permittivity $\underline{\epsilon}_{r2}$, one can use either the real part of $\underline{\epsilon}_{r2}$, ϵ'_{r2}, or the real part of the root square of $\underline{\epsilon}_{r2}$, $\Re e(\sqrt{\underline{\epsilon}_{r2}})$. Then, the refraction Snell–Descartes law (31) becomes, respectively

$$\sqrt{\epsilon'_{r2}} \sin \chi_t^{(1)} \simeq \sqrt{\epsilon_{r1}} \sin \chi_i, \tag{37}$$

$$\Re e(\sqrt{\underline{\epsilon}_{r2}}) \sin \chi_t^{(2)} \simeq \sqrt{\epsilon_{r1}} \sin \chi_i. \tag{38}$$

In the case of plane interfaces, the local angles χ can be denoted as θ. Here, for the numerical simulations, it is simpler to use the first approximation of the propagation angle, $\theta_t^{(1)} \simeq \theta_t^{\text{plane}}$, by replacing the complex permittivity $\underline{\epsilon}_{r2}$ with its real part ϵ'_{r2}. This approximation is less precise than the second one, but it is correct for weakly lossy media (more precisely, the precision depends on the incidence angle, the real part of the permittivity, ϵ'_{r2}, and the imaginary part of the permittivity; in general, even if ϵ'_{r2} tends to 1, for moderate incidence angles and weakly lossy media, the approximation is valid, and it is all the more precise as ϵ'_{r2} increases). For example, for a complex permittivity $\underline{\epsilon}_{r2} = 3 + 0.1i$ at an incidence angle $\theta_i = -20°$, the physical propagation angle is $\theta_t^{\text{plane}} = -11.3871°$, the first approximation obtained from equation (37) is $\theta_t^{(1)} = -11.3888°$, and the second approximation obtained from equation (38) is $\theta_t^{(2)} = -11.3872°$: both approximations are valid and precise. For $\underline{\epsilon}_{r2} = 3+i$ at $\theta_i = -20°$, $\theta_t^{\text{plane}} = -11.230°$, $\theta_t^{(1)} = -11.389°$, and $\theta_t^{(2)} = -11.236°$: both approximations are valid, but only the second one remains precise.

For the numerical simulations, the studied system is the same as in the first section, but with a layer of permittivity $\underline{\epsilon}_{r2} = 3+0.1i$. We consider two incidence angles $\theta_i = \{0°; -20°\}$. Then, the first approximation of the propagation angle, which replaces $\underline{\epsilon}_{r2} = 3+0.1i$ with its real part $\epsilon'_{r2} = 3$, can be used. With this approximation, one can obtain that the power propagation loss $\mathcal{A} \simeq \mathcal{A}_{pl} = 0.046 = -13.4$ dB for $\theta_i = 0°$, and $\mathcal{A} \simeq \mathcal{A}_{pl} = 0.041 = -13.9$ dB for $\theta_i = -20°$. The numerical simulations present a comparison of the lossy case ($\underline{\epsilon}_{r2} = 3 + 0.1i$), with the lossless case ($\epsilon_{r2} = 3$), and a comparison between the model with shadow, modified in order to take losses into account as described above, and the (reference numerical) PILE method. The simulations of the first-order contribution $\sigma_{r,1}$ for the lossy case are not plotted here. Indeed, for this configuration of weakly lossy medium, the difference with the lossless case can be ignored, as the modulus of the Fresnel reflection coefficient varies very slightly (the maximum of relative difference does not exceed 0.03%!).

Simulations of the contribution of $\sigma_{r,2}$ are presented for $\theta_i = 0°$ in figure 6, and for $\theta_i = -20°$ in figure 7. For the lossy case, the model with shadow is plotted as the dotted line, and the reference method in dashed line. Here, for these simulations, only the propagation loss $\mathcal{A}$ need to be considered in the model to quantify the lossy case. The lossless case is also plotted for comparison, together with the first-order contribution of the model with shadow (the lossless case, which is practically equal to the lossy case). For both incidence angles, for the two curves of the model with shadow (taking into account only the propagation loss) and of the reference numerical method, in both cases the difference between the lossy and the lossless case of the contribution of $\sigma_{r,2}$ is mainly constant, and is of the order of the planar propagation

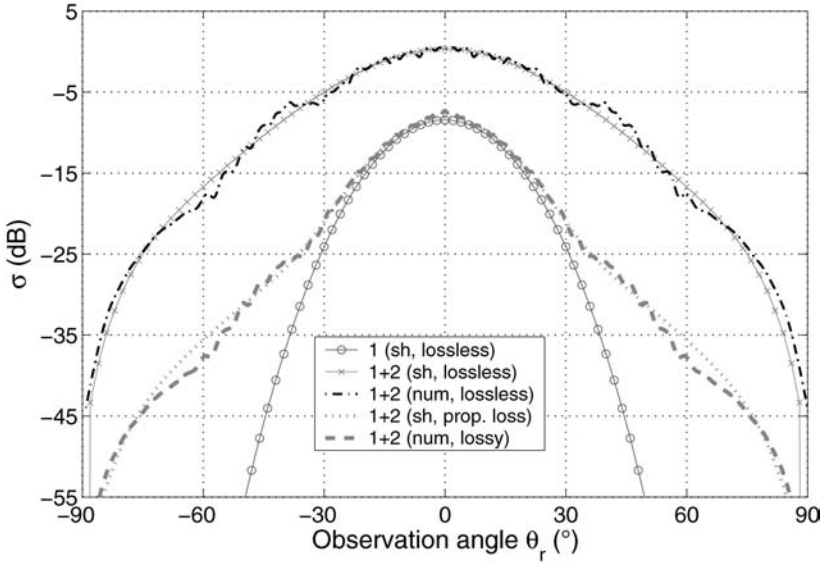

Figure 6. Simulations of the influence of a lossy inner medium of permittivity $\underline{\epsilon}_{r2} = 3 + 0.1i$ on the contribution of the second-order scattering coefficient $\sigma_{r,2}$ in dB, versus the reflection scattering angle θ_r (in $^\circ$) for V polarization, for $\epsilon_{r3} = i\infty$, and for $\theta_i = 0^\circ$: comparison of the case of a lossless inner medium of permittivity $\epsilon'_{r2} = \Re e(\underline{\epsilon}_{r2}) = 3$ (plotted as the crossed line for the model with shadow, and in dashdot line for the numerical model) with the case of a lossy inner medium of permittivity $\underline{\epsilon}_{r2} = 3 + 0.1i$ (plotted as the dotted line for the model with shadow, in which only the propagation loss is taken into account, and in dashed line for the numerical model). The first-order contribution is also plotted (circled line) for comparison.

loss ($\mathcal{A}_{pl} = 0.046 = -13.4$ dB for $\theta_i = 0^\circ$, and $\mathcal{A}_{pl} = 0.041 = -13.9$ dB for $\theta_i = -20^\circ$), calculated using equation (35). Moreover, for the lossy case, one can observe that the curves of the model with shadow (taking into account only the propagation loss) and the reference numerical model coincide around the specular direction $\theta_r = -\theta_i$, and the differences in other

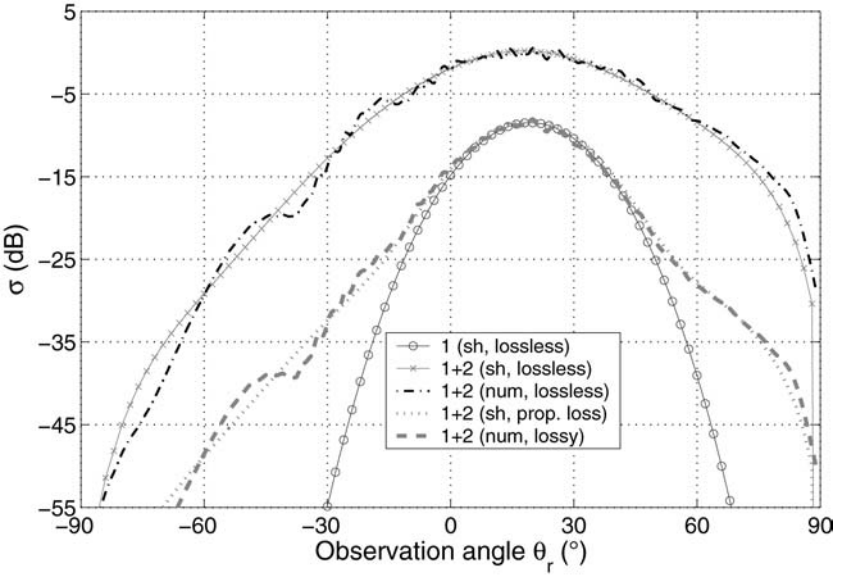

Figure 7. Same simulations as figure 6, but with $\theta_i = -20^\circ$.

configurations are the same as the ones observed for the lossless case, and can be attributed to the limitations of the numerical method.

Simulations for different values of $\underline{\epsilon}_{r2}$, with slight losses ($3 + 0.02i$ for example) have been done. They lead to the same results and conclusions, that is to say there is good agreement between the model with shadow (taking into account only the planar propagation loss) and the numerical method. This allows us to consider that for a configuration of slightly lossy media, the propagation loss is the main factor of losses, and quantitatively describes lossy inner media.

Thus, even though the studied model in itself cannot deal with lossy media, simple minor modifications to the model (mainly the addition of a propagation loss $\mathcal{A}$ into $\sigma_{r,2}$, which can be evaluated by considering plane interfaces) allow us to take this particular case into account, with good results.

8. Conclusion and discussion

The iteration of the KA is used to evaluate the electromagnetic scattering (in reflection and transmission) with shadow from a rough one-dimensional layer, for which successive reflections inside the rough layer are taken into account. The use of the shadowing function allows this method to be more precise at grazing angles, especially for high surface slope variances. The iterated KA is reduced to the high-frequency limit (which corresponds to very rough surfaces compared to the electromagnetic wavelength) to obtain numerical results. To our knowledge, it is the first time scattering coefficients are derived under the GO approximation for the case of several interfaces. The expressions of the scattering coefficients are given in closed-forms. Assuming that the points of successive reflections or transmission are uncorrelated between one another, they appear as the product of elementary scattering coefficients of single interfaces, corresponding to each reflection or transmission of the scattered wave inside the dielectric waveguide. The integrals account for the scattering directions from one scattering point to another. Under the GO approximation, the total scattering coefficient is obtained by incoherently adding the contributions of all orders. This model allows fast numerical results, as the calculation of the second-order contribution in reflection implies only two-fold integrations.

One can observe that the scattering coefficient can be applied for any given slope statistics, and is independent of the frequency (within the domain of validity of the model). The interest of this model is that the scattering coefficient in reflection, as well as in transmission, can be derived at any order for either a very rough or a plane lower interface. Indeed, expressions were given above for $\sigma_{r,1}$, $\sigma_{t,1}$ and $\sigma_{r,2}$, but they were also derived for any order of the scattering coefficient in reflection $\sigma_{r,n}$ or in transmission $\sigma_{t,n}$: for a rough lower interface and for a plane lower interface using the remark in subsection 3.2. (they are not presented here). Moreover, using the same approach, it is extendable to the superimposition of any number of very rough surfaces.

The studied model is validated by comparison with a benchmark numerical model [24, 25], based on the method of moments. The model can deal with a system made up of either a rough or a plane lower interface, with either a lossless or a lossy inner medium, for which simulations were presented. Moreover, slightly lossy inner media can be treated very simply by taking only the planar propagation loss into account. The model allows fast numerical results. Indeed, for given θ_i and θ_r, and with 40 sampling points for the numerical integrations over $\theta_{-,1}$ and $\theta_{+,1}$, the CPU time to calculate $\sigma_{r,1}$ and $\sigma_{r,2}$ is about 190 ms with a standard personal computer (500 MHz processor, 670 MB RAM), using MATLAB. The limitations of the model correspond to the limits of the Kirchhoff approximation in the high-frequency limit,

that is to say it is not valid for very small grazing angles, and it can only deal with surfaces with $\sigma_h >\sim 0.5\lambda$ (let us note that the simulations were lead for $\sigma_h = 0.5\lambda$ and allowed us to validate the model). With further investigations, it could be interesting to extend the model to the three-dimensional case to deal with general two-dimensional rough surfaces, using dyadic Green functions.

References

[1] Kaganovskii, Y., Freilikher, V., Kanzieper, E., Nafcha, Y., Rosenbluh, M., and Fuks, I., 1999, Light scattering from slightly rough dielectric films. *Journal of the Optical Society of America A*, **16**, 331–338.

[2] Knittl, Z., 1976, *Optics of Thin Films* (London: John Wiley).

[3] Eastman, J., 1978, Scattering by all-dielectric multilayer band-pass filters and mirrors for lasers. In: G. Hass and M. H. Francombe (Eds) *Physics of Thin Films*, Vol. 10, pp. 167–226 (New York: Academic Press).

[4] Ohlídal, I. and Navrátil, K., 1995, Scattering of light from multilayer with rough boundaries. In: E. Wolf (Ed.) *Progress in Optics*, Vol. XXXIV, pp. 248–331 (Amsterdam: Elsevier).

[5] Fuks, I. and Voronovich, A., 2000, Wave diffraction by rough interfaces in an arbitrary plane-layered medium. *Waves in Random Media*, **10**, 253–272.

[6] Soubret, A., Berginc, G., and Bourrely, C., 2001, Application of reduced Rayleigh equations to electromagnetic wave scattering by two-dimensional randomly rough surfaces. *Physical Review B*, **63**, 245411.

[7] Fuks, I., 2002, Modeling of scattering by a rough surface of layered media. In: 2002 IEEE International Geoscience and Remote Sensing Symposium, Toronto, Ontario, Canada, Vol. 2, pp. 1251–1253.

[8] Blumberg, D., Freilikher, V., Fuks, I., Kaganovskii, Y., Maradudin, A., and Rosenbluh, M., 2002, Effects of roughness on the retrorefiection from dielectric layers. *Waves in Random Media*, **12**, 279–292.

[9] Gu, Z.-H., Fuks, I., and Ciftan, M., 2004, Grazing angle enhanced backscattering from a dielectric film on a reflecting metal substrate. *Optical Engineering*, **43**, 559–567.

[10] Bahar, E. and Zhang, Y., 1999, Diffuse like and cross-polarized fields scattered from irregular layered structures-full-wave analysis. *IEEE Transactions on Antennas and Propagation*, **47**, 941–948.

[11] Zhang, Y. and Bahar, E., 1999, Mueller matrix elements that characterize scattering from coated random rough surfaces. *IEEE Transactions on Antennas and Propagation*, **47**, 949–955.

[12] Tjuatja, S., Fung, A., and Dawson, M., 1993, An analysis of scattering and emission from sea ice. *Remote Sensing Reviews*, **7**, 83–106.

[13] Fung, A. and Pan, G., 1986, An integral equation method for rough surface scattering. In: Proceedings of the International Symposium on Multiple Scattering of Waves in Random Media and Random Surfaces, Pennsylvania State University, pp. 701–714.

[14] Fung, A., 1994, *Microwave Scattering and Emission Models and Their Applications* (Boston: Artech House).

[15] Beckmann, P. and Spizzichino, A., 1963, *The Scattering of Electromagnetic Waves from Rough Surfaces* (Oxford: Pergamon Press).

[16] Ogilvy, J., 1991, *Theory of Wave Scattering from Random Surfaces* (Bristol: Institute of Physics Publishing).

[17] Kong, J. A., 1990, *Electromagnetic Wave Theory*, 2nd edn (New York: John Wiley).

[18] Caron, J. Lafait, J., and Andraud, C., 2002, Scalar Kirchhoff model for light scattering from dielectric random rough surfaces. *Optics Communications*, **207**, 17–28.

[19] Bahar, E. and El-Shenawee, M., 2001, Double-scatter cross sections for two-dimensional random rough surfaces that exhibit backscatter enhancement. *Journal of the Optical Society of America A*, **18**, 108–116.

[20] Ishimaru, A., Le, C., Kuga, Y., Sengers, L., and Chan, T., 1996, Polarimetric scattering theory for high slope rough surfaces. *Progress in Electromagnetic Research*, **14**, 1–36.

[21] Bourlier, C. and Berginc, G., 2004, Multiple scattering in the high-frequency limit with second-order shadowing function from 2D anisotropic rough dielectric surfaces: I. Theoretical study. *Waves in Random Media*, **14**, 229–252.

[22] Bourlier, C., Berginc, G., and Saillard, J., 2002, Monostatic and bistatic statistical shadowing functions from a one-dimensional stationary randomly rough surface according to the observation length: I. Single scattering. *Waves in Random Media*, **12**, 145–173.

[23] Pinel, N., Bourlier, C., and Saillard, J., 2005, Energy conservation of the scattering from rough surfaces in the high-frequency limit. *Optics Letters*, **30**, 2007–2009.

[24] Déchamps, N., 2004, Méthodes numériques appliquées au calcul de la diffusion d'une onde électromagnétique par des interfaces naturelles monodimensionnelles. PhD thesis, Université de Nantes, Nantes, France.

[25] Déchamps, N. de Beaucoudrey, N. Bourlier, C., and Toutain, S., 2006, Fast numerical method for electromagnetic scattering by rough layered interfaces: Propagation-inside-layer expansion method. *Journal of the Optical Society of America A*, **23**, 359–369.

[26] Tsang, L., Kong, J., Ding, K., and Ao, C., 2000, *Scattering of Electromagnetic Waves, Volume I: Theories and Applications* (New York: John Wiley).

[27] Tsang, L. and Kong, J., 2001, *Scattering of Electromagnetic Waves, Volume III: Advanced Topics* (New York: John Wiley).

[28] Bruce, N., 2004, On the validity of the inclusion of geometrical shadowing functions in the multiple-scatter Kirchhoff approximation. *Waves in Random Media*, **14**, 1–12.

[29] Sancer, M., 1969, Shadow-corrected electromagnetic scattering from a randomly rough surface. *IEEE Transactions on Antennas and Propagation*, **AP-17**, 577–585.
[30] Tsang, L., Kong, J. A., Ding, K. H., and Ao, C. O., 2001, *Scattering of Electromagnetic Waves, Volume II: Numerical Simulations* (New York: John Wiley).
[31] Fung, A., Li, Z., and Chen, K., 1992, 'Backscattering from a randomly rough dielectric surface. *IEEE Transactions on Geoscience and Remote Sensing*, **30**, 356–369.
[32] Jakeman, E., 1988, 'Enhanced backscattering through a deep random phase screen. *Journal of the Optical Society of America A*, **5**, 1638–1648.
[33] Lu, J., Maradudin, A., and Michel, T., 1991, Enhanced backscattering from a rough dielectric film on a reflecting substrate. *Journal of the Optical Society of America B*, **8**, 311–318.
[34] Pinel, N., Bourlier, C., and Saillard, J., 2005, Radar cross section from a stack of two one-dimensional rough interfaces in the high-frequency limit. In: European RADar 2005 Symposium, European Microwave Association, Paris, France.
[35] Harrington, F., 1993, *Field Computation by Moment Methods* (IEEE Press).
[36] Bourlier, C. and Berginc, G., 2004, Multiple scattering in the high-frequency limit with second-order shadowing function from 2D anisotropic rough dielectric surfaces: II. Comparison with numerical results. *Waves in Random Media*, **14**, 253–276.
[37] Lynch, P. and Wagner, R., 1970, Rough-surface scattering: shadowing, multiple scatter, and energy conservation. *Journal of Mathematical Physics*, **11**, 3032–3042.
[38] Saillard, M. and Toso, G., 1997, Electromagnetic scattering from bounded or infinite subsurface bodies. *Radio Science*, **32**, 1347–1360.
[39] Nghiem, S., Kwok, R., Yueh, S., and Drinkwater, M., 1995, Polarimetric signatures of sea ice. 1. Theoretical model. *Journal of Geophysical Research*, **100**, 13665–13679.
[40] Nghiem, S., Kwok, R., Yueh, S., and Drinkwater, M., 1995, Polarimetric signatures of sea ice. 2. Experimental observations. *Journal of Geophysical Research*, **100**, 13681–13698.
[41] Lu, J., Hu, X.-H., and Dong, K., 2000, Modeling of the rough-interface effect on a converging light beam propagating in a skin tissue phantom. *Applied Optics*, **39**, 5890–5897.
[42] Ripoll, J., Ntziachristos, V., Culver, J., Pattanayak, D., Yodh, A., and Nieto-Vesperinas, M., 2001, Recovery of optical parameters in multiple-layered diffusive media: theory and experiments. *Journal of the Optical Society of America A*, **18**, 821–830.
[43] Croce, P. and Prod'homme, L., 1980, Contribution of immersion technique to light scattering analysis of very rough surfaces. *Journal of Optics*, **11**, 319–327.
[44] Croce, P. and Prod'homme, L., 1984, On the conditions for applying light scattering methods to rough surface evaluation. *Journal of Optics*, **15**, 95–104.
[45] Yin, Z., Tan, H., and Smith, F., 1996, Determination of the optical constants of diamond films with a rough growth surface. *Diamond and Related Materials*, **5**, 1490–1496.
[46] Yin, Z., Akkerman, Z., Yang, B., and Smith, F., 1997, Optical properties and microstructure of CVD diamond films. *Diamond and Related Materials*, **6**, 153–158.
[47] Stagg, B. and Charalampopoulos, T., 1991, Surface-roughness effects on the determination of optical properties of materials by the reflection method. *Applied Optics*, **30**, 4113–4118.
[48] Combes, P.-F. Micro-ondes – Cours et exercices avec solutions. Tome 1: Lignes, guides et cavités. Dunod, 1996.
[49] Roo, R. D. and Tai, C.-T., 2003, Plane wave reflection and refraction involving a finitely conducting medium. *IEEE Antennas and Propagation Magazine*, **45**, 54–61.